Journal of Medicinal Chemistry

Article

Discovery of Novel and Highly Selective Inhibitors of Calpain for the Treatment of Alzheimer´s Disease: 2-(3-Phenyl-1H-pyrazol-1-yl)nicotinamides

Andreas Kling, Katja Jantos, Helmut Mack, Wilfried Hornberger, Karla Drescher, Volker Nimmrich, Ana Relo, Karsten Wicke, Charles W. Hutchins, Yanbin Lao, Kennan C Marsh, and Achim Moeller

J. Med. Chem., **Just Accepted Manuscript** • DOI: 10.1021/acs.jmedchem.7b00731 • Publication Date (Web): 31 Jul 2017

Just Accepted

ACS Publications

Journal of Medicinal Chemistry is published by the American Chemical Society. 1155 Sixteenth Street N.W., Washington, DC 20036

Discovery of Novel and Highly Selective Inhibitors of Calpain for the Treatment of Alzheimer´s Disease: 2-(3-Phenyl-1H-pyrazol-1-yl)-nicotinamides

Andreas Kling,[†,] Katja Jantos,[†] Helmut Mack,[†] Wilfried Hornberger,[†] Karla Drescher,[†,#] Volker Nimmrich,[†,⊥] Ana Relo,[†] Karsten Wicke,[†] Charles W. Hutchins,[‡] Yanbin Lao,[‡,#,⊥] Kennan Marsh,[‡] Achim Moeller[†,#]*

†AbbVie Deutschland GmbH & Co. KG, Neuroscience Research, Knollstrasse, 67061 Ludwigshafen, Germany

‡AbbVie Inc., 1 North Waukegan Road, North Chicago, Illinois 60064-6125, United States of America

ABSTRACT: Calpain overactivation has been implicated in a variety of pathological disorders including ischemia/reperfusion injury, cataract formation, and neurodegenerative diseases such as Alzheimer´s Disease (AD). Herein we describe our efforts leading to the identification of ketoamide-based 2-(3-phenyl-1H-pyrazol-1-yl)nicotinamides as potent and reversible inhibitors of calpain with high selectivity versus related cysteine protease cathepsins, other proteases and

receptors. Broad efficacy in a set of preclinical models relevant to AD suggests that inhibition of calpain represents an attractive approach with potential benefit for the treatment of AD.

INTRODUCTION AND RATIONALE

The calpains are a family of proteases that are constitutively expressed in the inactive form, some of which are activated by Calcium.[1,2] Calpain 1 and 2 belong to the Ca2+-activated calpains and together with calpains 3, 8, 9 constitute a subfamily of cysteine proteases that are responsible for limited proteolysis of a variety of target substrates. The two isoforms, calpain 1 and 2, differ in their Ca2+-sensitivities required for activation and are expressed ubiquitously, whereas the other members of the subfamily show a tissue specific expression pattern. The activity of calpain 1 and 2 is tightly controlled by the natural specific protein inhibitor calpastatin, which only binds to activated calpains. Under physiological conditions calpains are involved in processes like cytoskeletal remodeling, modulation of signal transduction pathways, platelet activation, cell differentiation and apoptotic cell death. Overactivation of both calpain 1 and calpain 2 results in unregulated proteolysis and aberrant activation of signaling cascades, leading to cellular damage and ultimately to cell death. Inhibition of calpain after pathological insult has been shown to exert general cell- and organ-protective effects. Therefore calpain has been proposed as attractive target for several human pathological disorders such as chronic kidney disease, ischemia/reperfusion injury, cataract formation, and neurological diseases.[3,4] Recent evidence suggests that disruption of calcium homeostasis in neuronal cells leads to a dysregulation of calpain. Activated calpain 1 and 2 have been found in plaques and neurofibrillary tangles of the brain of Alzheimer´s Disease (AD) patients, and are critically involved in the multiple pathogenic processes of AD.[5-7] Calpains modulate processes that regulate the function of proteins key to the pathogenesis of AD, such as dynamin-dependent

synaptic signaling, cytoskeletal turnover and remodeling.[8-11] In addition, calpain is part of the NMDA-dependent excitoxic cascade[12,13] and modulates the activity of protein kinases such as CDK5, which play a role in tau pathology, Aβ generation, and dysregulation of mitochondrial function. All of these events lead to impaired synaptic function, neuroinflammation/degeneration and finally neuronal death.[14,15] Inhibition of calpain (via overexpression of the natural inhibitor calpastatin) was shown to restore synaptic function and prevent neurodegeneration in different transgenic mouse models related to AD, whereas overexpression of calpain promoted amyloid plaque formation and neuronal degeneration.[16-18]

In summary, these findings suggest that inhibition of calpain 1 and 2 is a compelling approach to address synaptic dysfunction and neurodegeneration, and that an appropriate calpain inhibitor could have therapeutic potential for the treatment of neurodegenerative diseases like AD.[19-21]

Calpain inhibitors: The majority of calpain inhibitors described so far are active site directed and can be grouped into reversible and irreversible inhibitors. A common feature of these inhibitors is the presence of an electrophilic center, which is required for covalent interaction with the catalytic cysteine residue of the protease. Residues on the adjacent sides of the warhead interact with pockets at the subsites of calpain in a manner similar to substrate binding with most inhibitors presenting their backbones in a β-strand conformation (**Figure 1**).

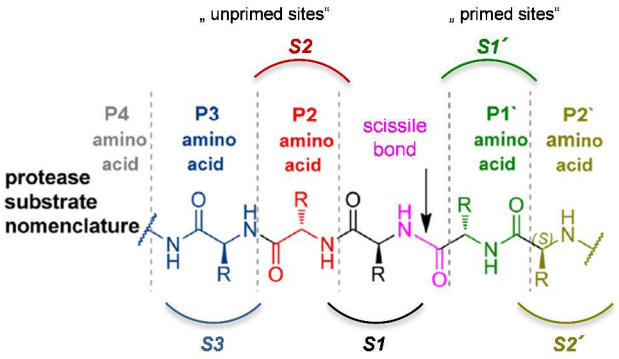

Figure 1 Protease substrates are designated according to their residues extending from the scissile bond. Backbone side chains P3 to P2´ are supposed to interact with the corresponding protease sub sites S3 to S2´ (*adapted from lit. 24*).

Over the past decades many groups have been engaged in the field of calpain inhibitors, and corresponding patent applications and scientific literature have been extensively reviewed.[22-25] Although a variety of potent calpain inhibitors has been disclosed, none of these compounds were suitable for further advancement into clinical development. Major limitations were the lack of specificity versus other proteases and the proteasome, low cellular penetration, limited metabolic stability and no or insufficient bioavailability. In 2003, we disclosed a series of non-peptidic ketoamide-based calpain inhibitors comprising an ortho-substituted benzoyl residue in the P2 position.[26] Analogues from this series were potent inhibitors of calpain 1 and 2 with Ki values in the nanomolar range, selectivity versus the proteasome, high cell permeability, water solubility, oral bioavailability and were shown to exert protective effects in several organ injury models.[27-29]

In particular, *N*-(1-benzyl-2-carbamoyl-2-oxo-ethyl)-2-[(E)-2-(4-diethylaminomethylphenyl)-vinyl]benzamide **1** (**A-705253**) has emerged as prototypic calpain inhibitor and was used by us and others as a tool compound to demonstrate efficacy in AD-relevant animal models covering synaptic dysfunction, neurodegeneration and tau hyperphosphorylation.[30-34] Furthermore, chronic

administration of **1** in aged 3xTg mice significantly mitigated the AD-like pathology and cognitive decline.[35] Altogether, these data strongly support our hypothesis that inhibition of calpain might present a promising novel approach for the treatment of AD.

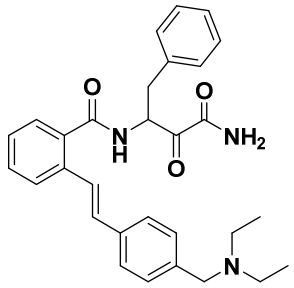

1

Ki Cal 1= 56 nM
Ki Cat B= 28 nM, Cat K= 1.8 nM,
Cat L= 137 nM, Cat S= 3290 nM
Inhibition at 10μM:
Cat C= 94%, Cat H= 84%

Figure 2 Structure and *in-vitro* inhibition profile of compound **1**

Although compound **1** is a highly efficacious calpain inhibitor, its lack of selectivity versus the related cysteine protease cathepsins B, K, L, S, and C prevented further advancement of the compound (**Figure 2**). Analysis of the physiological and pathological functions of cysteine protease cathepsins revealed that inhibition of cathepsin C and in particular L and S is expected to result in immunosuppression as side effect. In contrast, inhibition of cathepsins B and K at supra-efficacious exposure levels is not considered detrimental.[36-40] We concluded that high selectivity versus cathepsins L, S and C is indispensable, whereas moderate selectivity versus cathepsins B and K might be tolerable.

Therefore, our objective was to identify novel calpain inhibitors with enhanced selectivity starting from **1** as a lead. Initial efforts were focused on exploring the P3-P2 linker to address the inherent light-sensitivity observed for this chemotype, which probably originates from the presence of the stilbene unit. Comparison of **1** with pyridyl analogue **2** revealed that introduction of N in P2 has a positive impact on cathepsin S selectivity while only slightly affecting calpain potency (**Scheme 1)**. Parallel studies on a related chemotype showed that introduction of

piperazine or pyrrolidine as P3-P2 linker in combination with P2 nicotinamide and phenyl in P3 (compounds **3** and **4**) also led to calpain inhibitors with Ki values in range comparable to **1**.[41] Based on these results we considered an alternative approach towards novel calpain inhibitors: replacement of P3-P2 vinyl by 5-member hetaryl should mimic the conformational constraint of the stilbene unit and retain the overall orientation of phenyl towards the hydrophobic P3 pocket of the enzyme.

Scheme 1 Starting points for optimization[a]

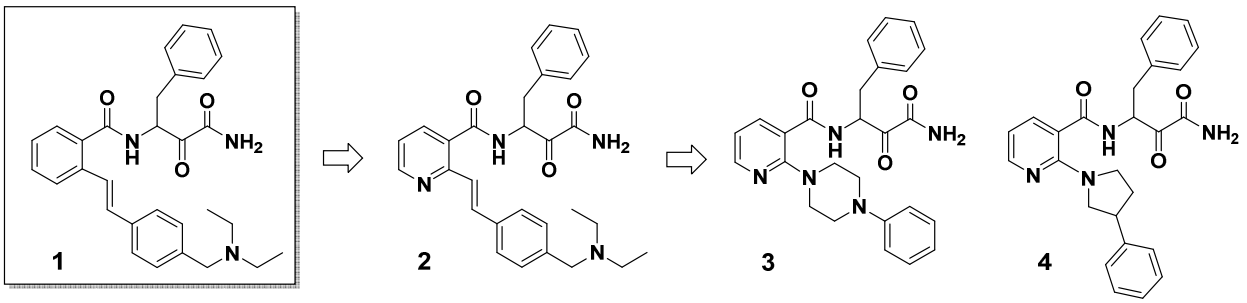

	1	2	3	4
Ki Cal 1=	56 nM	109 nM	250 nM	125 nM
Cat L=	137 nM	204 nM	491 nM	39 nM
Cat S=	3290 nM	> 10.000 nM	7260 nM	1780 nM

[a]Tested as racemates.

Herein we describe the identification and synthesis of *N*-(4-amino-3,4-dioxo-1-phenylbutan-2-yl)-2-(3-phenyl-1*H*-pyrazol-1-yl)nicotinamide **19** (**A-933548**) as a potent and selective inhibitor of calpain. Compound **19** and analogues feature enhanced selectivity versus related cysteine protease cathepsins, favorable microsomal stability and efficacy in cellular assays. Selected compounds such as 4-fluoro derivative *N*-(4-amino-3,4-dioxo-1-phenylbutan-2-yl)-2-(3-(4-fluorophenyl)-1*H*-pyrazol-1-yl)nicotinamide **38** (**A-953227**) were advanced further and

characterized for PK properties and preclinical safety profile. In addition, compound **38** was also shown to reproduce the *in-vivo* profile demonstrated with **1** in AD-related models.

RESULTS AND DISCUSSION

Synthesis: **Scheme 2** outlines the synthesis of *N*-(4-amino-3,4-dioxo-1-phenylbutan-2-yl)-2-((3-phenyl-1H-pyrazol-1-yl)nicotinamide **19** as general example for the synthesis of compounds **17-45** comprising different P3-P2 hetaryl linkers. Starting from ethyl 2-chloronicotinate, nucleophilic substitution using 3-phenyl-1H-pyrazole led to ethyl 2-(3-phenyl-1H-pyrazol-1-yl)nicotinate **5**. Ester cleavage and coupling with 3-amino-2-hydroxy-4-phenylbutanamide yielded the corresponding hydroxyamide intermediate *N*-(4-amino-3-hydroxy-4-oxo-1-phenylbutan-2-yl)-2-(3-phenyl-1H-pyrazol-1-yl)nicotin- amide **7**, which in the final step was oxidized using Pfitzner-Moffat conditions[42] to give ketoamide **19**. Final compounds **17–45** were prepared as outlined for **19** starting from the appropriate P3-P2 acids, and were provided as racemic mixtures (unless noted otherwise).

Scheme 2 Synthetic route to *N*-(4-amino-3,4-dioxo-1-phenylbutan-2-yl)-2-((3-phenyl-1H-pyrazol-1-yl)nicotinamide **19** and analogues [a]

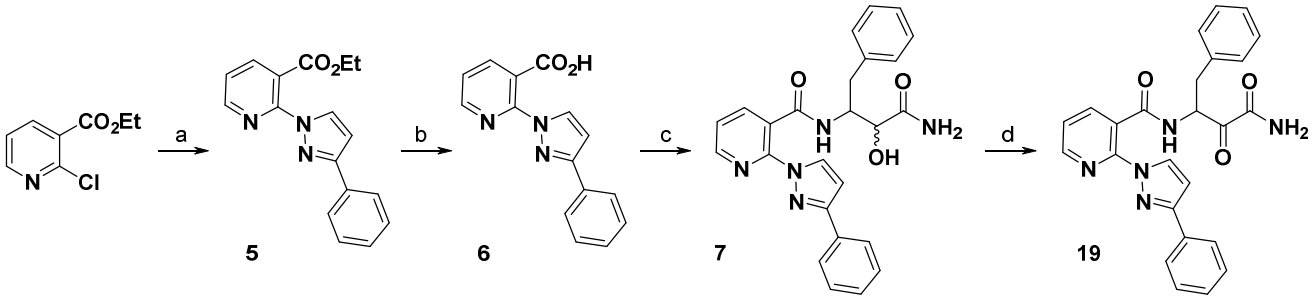

[a]Reagents and conditions: a) 3-phenyl-1H-pyrazole, K_2CO_3, KI, DMF, 130°C; b) NaOH, MeOH/H_2O, rt.; c) 3-amino-2-hydroxy-4-phenylbutanamide, EDCI, HOBt, triethlyamine, CH_2Cl_2, 0°C – rt.; d) EDCI, dichloroacetic acid, DMSO, rt.

Substituted pyrazoles employed in the synthesis were either commercially available or prepared as exemplified for the diethylamino- and morpholinobenzyl analogue **8** in **Scheme 3**. Condensation of appropriate phenylethan-2-ones with DMF dimethylacetal under microwave conditions gave the corresponding 1-aryl-3-dimethylamino-2-propen-1-ones, which upon treatment with hydrazine hydrate were converted into the 3-substituted pyrazoles.[43]

Scheme 3 Synthetic route to 4-methylaminosubstituted 3-phenyl-1*H*-pyrazoles **8**[a]

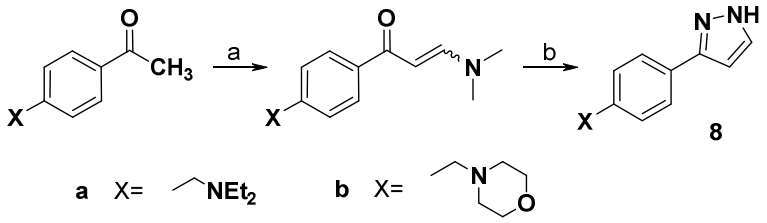

[a]Reagents and conditions: a) DMF dimethylacetal, reflux; b) N_2H_4 x H_2O, MeOH, reflux.

2-(2-Phenylthiazol-4-yl)- and 2-(4-phenylthiazol-2-yl)nicotinic acid **9** and **11** were prepared via classical Hantzsch thiazole synthesis (**Scheme 4**).[44] Thus, methyl 2-acetyl-nicotinate was converted into the α-bromo analogue and reacted with benzothioamide to give thiazole **9**. Analogous reaction using the commercially available ethyl 2-carbamothioylnicotinate and 2-bromo-1-phenylethan-1-one led to 4-phenyl-substitued thiazole **11**. Synthesis of 2-(2-phenyloxazol-4-yl)nicotinic acid **14** was achieved via Suzuki-Miyaura[45] cross coupling of ethyl 2-chloronicotinate and 2-phenyl-4-(4,4,5,5,-tetramethyl-1,3,2-dioxaborolan-2-yl)oxazole to give **13**. Ester cleavage then gave the desired nicotinic acid analogues **10**, **12** and **14**, which were reacted further as described for the synthesis of compound **19**.

Scheme 4 Synthetic route to 2- and 4-phenylthiazolyl-substituted nicotinic acid derivatives **10** and **12** and 2-phenyloxazolyl-analogue **14** [a]

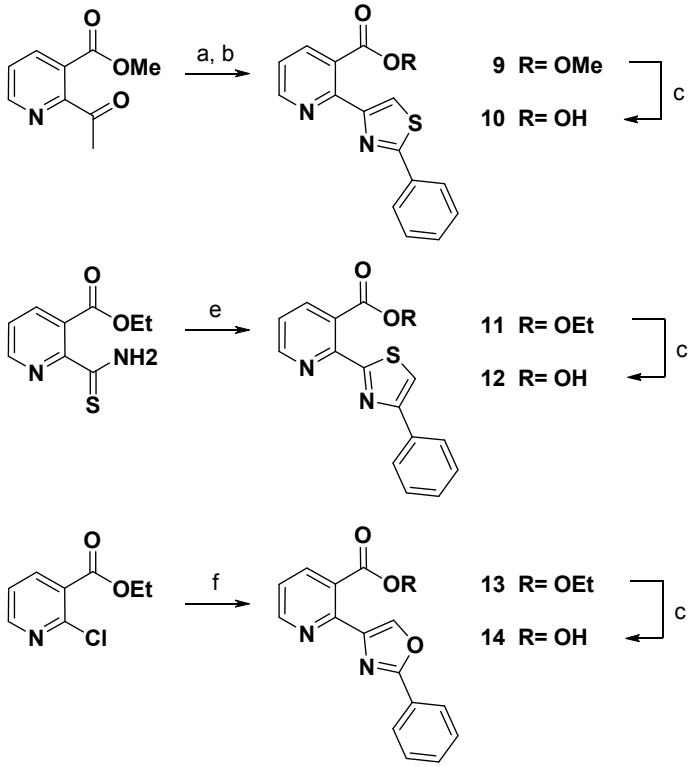

[a]Reagents and conditions: a) $PyBr_3$, HBr/HOAc, rt; b) benzothioamide, DMF, rt.; c) NaOH, $MeOH/H_2O$, rt; e) 2-bromo-1-phenylethan-1-one, DMF, rt; f) 2-phenyl-4-(4,4,5,5,-tetramethyl-1,3,2-dioxaborolan-2-yl)oxazole, PEPPSI-IPr, K_2CO_3, dioxane, 65°C.

The P1 building blocks commonly employed, 3-amino-2-hydroxy-4-phenylbutanamide and 3-amino-2-hydroxyheptanamide, were prepared according to literature procedures.[26,46] (3*S*)- and (3*R*)-3-amino-2-hydroxy-4-phenylbutanamide with defined configuration at the P1 stereogenic center were prepared following a route described by Pellacini et al.[47] Benzyloxycarbonyl-protected (*S*)- or (*R*)-2-amino-3-phenylpropan-1-ol was oxidized to the aldehyde and directly converted into the corresponding cyanohydrin (**Scheme 5**). Hydrolysis to amides **15a** and **b** and hydrogenolytic cleavage of the protecting group yielded the envisaged P1 hydroxyamides, which

were employed in the synthesis of compounds *(S)*- and *(R)*-**19**, respectively. Optical purity of the final products was monitored via chiral HPLC.

Scheme 5 Preparation of (2*R*, 3*S*)-3-amino-2-hydroxy-4-phenylbutanamide **16a** [a]

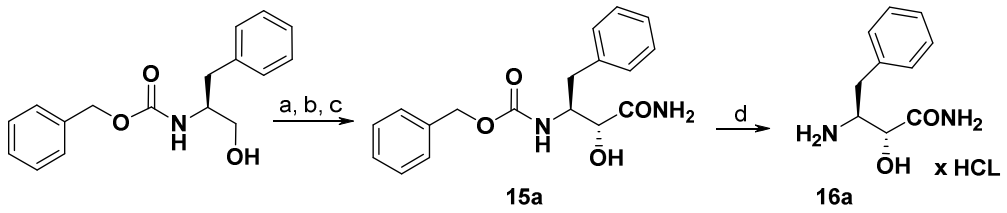

[a]Reagents and conditions: a) DMSO, oxalylchloride, CH_2Cl_2, -70°C - rt.; b) trimethylsilyl-cyanide, THF, rt.; c) conc. HCl, dioxane, 10°C – rt.; d) H_2, Pd-C, MeOH, rt.

Screening: Compounds **17 - 45** were evaluated for enzyme inhibition using kinetic fluorescence assays. Primary activity screening was performed using natural human calpain 1 isolated from human erythrocytes. Detailed structural analysis of related cysteine protease families revealed cathepsins B, K, L and S as closest active site homologues of calpain, hence selectivity for these cathepsins was assessed routinely (**Table 1-4**). Cellular efficacy was determined by measuring a compounds ability to prevent NMDA-induced cleavage of the calpain substrate spectrin into the corresponding spectrin degradation products (SDP 150 kDa and SDDP 145 kDa) in rat hippocampal slice cultures. In addition, all compounds were routinely submitted to ADME tier 1 screening comprising rat and human microsomal stability and cell permeability.

SAR: As outlined above, we started exploring various phenyl-substituted hetaryl linkers in P3-P2 position in combination with P2 pyridyl (**Table 1**). Whereas 1,4- and 1,3-substituted pyrazoles **18** and **19**, respectively, displayed enhanced calpain potency, 1,3-substituted imidazole **17** and 2,4-substituted thiazole **20** showed inhibition of calpain in a range comparable to **1**. The corresponding oxazole analogue **21** and the isomeric thiazole **22** showed 4-5 fold reduced

potency. In terms of selectivity only 1,3-substituted pyrazole **19** and 2,4-substituted thiazole **20** had the desired selectivity profile with high selectivity versus cathepsins S and L and moderate versus cathepsins B and K.

Table 1. Inhibition of calpain 1 and cathepsin selectivity for compounds **17 – 24**

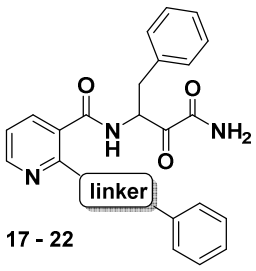

17 - 22

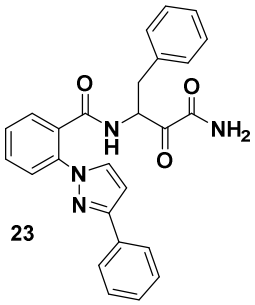

23

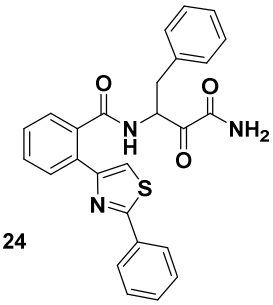

24

			--- selectivity ratios Cat/Cal ---			
compd	linker	Cal 1 Ki [nM]	CatB	CatK	CatL	CatS
1	-	56	< 1	< 0.1	2.5	59
17		45	< 1	< 1	23	54
18		21	< 1	1	12	14
19		18	26	21	176	>500
20		38	39	11	139	310
21		177	11	20	29	127
22		234	10	11	37	105
23	-	43	7	1	38	82
24	-	82	23	< 1	116	186

Investigation of the corresponding P2 phenyl analogues **23** and **24** confirmed the positive impact of pyridyl in P2 position. Both compounds showed diminished cathepsin selectivitity, in particular for cathepsin K. However, in the case of thiazole **24** the observed changes in selectivity for cathepsins B, L and S are mainly caused by the reduction in calpain potency, since the absolute Ki values for these cathepsins are similar between **24** and **20**. For selected examples we examined the impact of P1 variation and prepared the respective *N*-(1-amino-1,2-dioxoheptan-3-yl)nicotinamides comprising n-butyl as P1 side chain (**Table 2**). Compounds **25-27** retained inhibition of calpain in a range comparable to the P1 benzyl analogues **17-19**, whereas thiazole **28** displayed a 3 fold reduction in potency. However, cathepsin selectivity was found to be significantly reduced for all of these analogues and not in an acceptable range. Further exploration of the SAR for P1 revealed that P1 benzyl remained optimal in terms of selectivity profile (*data not shown).*

Table 2. Inhibition of calpain 1 and cathepsin selectivity for compounds **25 - 28**

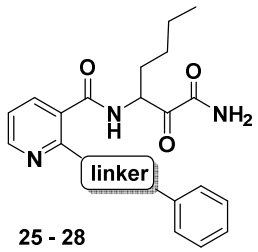

25 - 28

			--- selectivity ratios Cat/Cal ---			
compd	linker	Cal 1 Ki [nM]	CatB	CatK	CatL	CatS
25		38	< 1	< 1	22	22
26	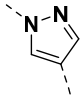	20	< 1	< 1	4	2
27	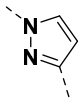	32	1	2	25	61
28		122	2	1	13	27

To better understand the structural basis of the SAR for inhibitors **17-28** a homology model of human calpain 1 was developed using the crystal structure of leupeptin in rat calpain as template.[48] Superposition placed the ketoamide-based inhibitors in the binding cleft in a pose comparable to leupeptin, with the P2 pyridine fitting well into the S2 site and the phenyl-substituted 5-member heterocycle into S3. For the selected human cathepsins the compounds could be modeled into similar poses. Potency and selectivity of the various ligands investigated can be explained primarily by the differences between calpain and cathepsins in the S3 and the S1 region, this is depicted using compound **19** as representative (**Figure 3**).

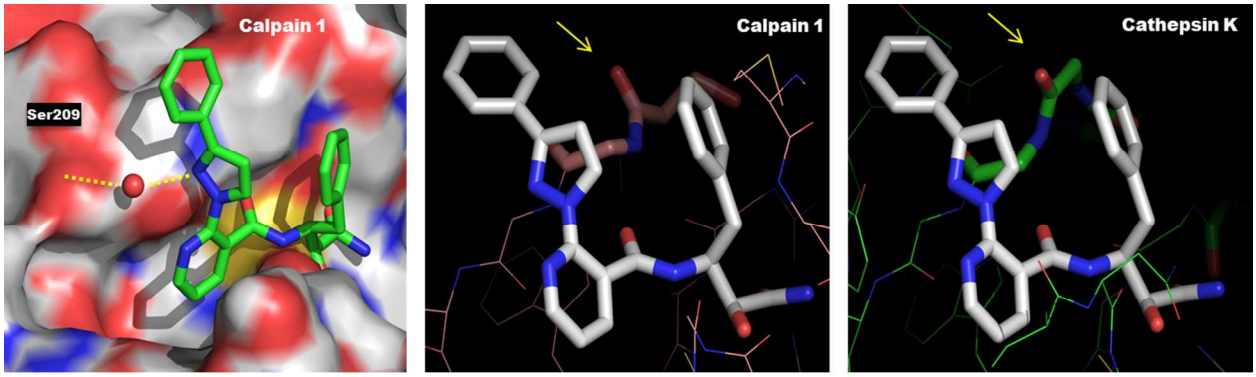

Figure 3 Model of compound **19** in the active site of human calpain 1 and cathepsin K.[48,49] *Left*: Surface model of calpain 1 with **19** in the active cleft; shown is the postulated water-mediated interaction between S3 Ser209 and P3 pyrazole N. *Center and Right*: Close-up on S1: in calpain P1 phenyl aligns in parallel to Gly207/Ser208 amide (center), whereas in cathepsin K (right) the corresponding amide carbonyl is rotated about 90° towards the phenyl residue.

In general, in the distant part of the S3 site the secondary structure of calpain differs from the cathepsins: whereas calpain 1 has an open pocket in this region, the cathepsin backbone forms a β-strand (*see Supporting Information*). Therefore substituents at the P3 hetaryl residue are expected to show an impact on overall selectivity. In addition, the pyrazole N in compound **19** is able to form a water-mediated hydrogen bond with Ser209 at the S3 site of calpain, thereby contributing to the overall binding affinity of this molecule (**Figure 3** *left*). This hypothesis is supported by the fact that all hetaryl residues with N in this position show selectivity. In contrast, the cathepsins studied have larger residues in this position (Tyr for cathepsins B and K, Leu for cathepsin L, and Phe for cathepsin S), which are not able to form stabilizing interactions.

In addition, at the S1 site in calpain 1 the P1 phenyl residue in **19** aligns parallel with the backbone amide at Gly207 in an amide-π interaction, and thus fits well into this sub pocket

(**Figure 3** *center*). The cathepsins show a different folding of the backbone in this region with the corresponding amide carbonyl rotated towards the P1 phenyl, which leads to an unfavorable interaction and thus contributes to selectivity. (**Figure 3** *right,* cathepsin K depicted as example). When changing P1 from benzyl to n-butyl, the alkyl side chain is able to rotate torsions to interact well with both the calpain or the cathepsin backbone amide, which explains the loss of selectivity for this P1 modification, while calpain potency is retained.

Based on the data obtained we focused our efforts on pyrazole **19** and moved on to further explore the SAR for P3. **Table 3** summarizes the results obtained. As expected, omitting P3 substitution led to significant reduction in calpain inhibition (compound **29**). We then evaluated whether non-aryl substituents in P3 would be tolerated, since this modification was also supposed to enhance the fraction sp^3, which for compound **19** is not in an optimal range.[50] In terms of calpain inhibition, P3 benzyl derivative **35** exhibited the highest potency, followed by cyclohexyl and tetrahydropyranyl analogues **30** and **33**, respectively. The latter two derivatives also showed significantly enhanced fraction sp^3. However, none of the analogues **29-36** could compete with compound **19** in terms of calpain potency and selectivity profile.

Table 3. Inhibition of calpain 1 and cathepsin selectivity for compounds **29 – 36**

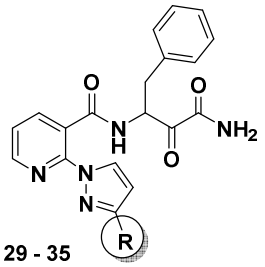

29 - 35

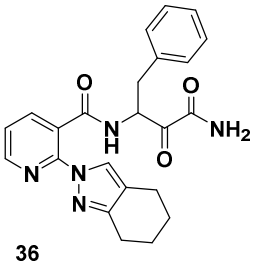

36

compd	R	Cal 1 Ki [nM]	--- selectivity ratios Cat/Cal -- CatB	CatK	CatL	CatS	fsp^3
19	-	18	26	21	176	>500	0.08
29	H	164	1	3	20	21	0.11
30		56	9	10	33	92	0.32
31		81	16	24	10	56	0.26
32		94	4	7	34	50	0.23
33	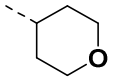	48	14	13	56	147	0.29
34	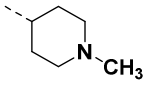	146	2	1	2	89	0.32
35	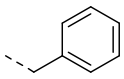	38	9	9	50	75	0.12
36	-	101	2	2	45	10	0.26

Subsequently, we explored substitution at P3 phenyl, with **Table 4** presenting the results for selected examples. Introduction of chloro, methoxy and trifluoromethyl in 4-position (**37**, **39** and **40**) led to diminished calpain inhibition, whereas 4-fluoro analogue **38** and 3-trifluoromethyl derivative **41** retained calpain potency and the overall selectivity profile, although with varied

selectivities for the individual cathepsins. As demonstrated by indazole **44**, annelation of P3 phenyl also resulted in reduced selectivity, most notably in the case of cathepsin S. In analogy to the structure of compound **1** we also explored the impact of additional basic moieties in P3. Benzyldiethylamine **42** and its respective morpholine analogue **43** were both found to act as nonselective inhibitors of calpain and cathepsins B, K and L with moderate to favorable selectivity versus cathepsin S, respectively. Remarkably, chromene analogue **45** represented the most potent calpain inhibitor from this series and also featured the highest cathepsin selectivity. However, the extremely low solubility of **45** in aqueous and non-aqueous vehicles prevented us from further advancing this compound.

Selected derivatives were submitted to screening for cellular efficacy. As depicted in **Table 4** compounds **19** and **38** showed the highest efficacy in a functional cellular assay using prevention of NMDA-induced intracellular spectrin cleavage as read-out. Both compounds have IC_{50} values in a range comparable to **1** (rat HSC IC_{50}= 461 nM total and 36 nM free).

Table 4. Inhibition of calpain 1 and cathepsin selectivity for compounds **37 – 45**

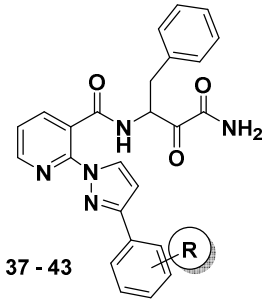

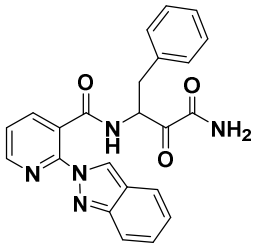

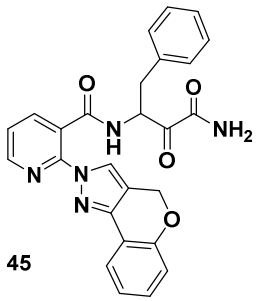

			---- selectivity ratios Cat/Cal ---				
compd	R	Cal 1 Ki [nM]	CatB	CatK	CatL	CatS	rat HSC[a] IC_{50} [nM] total/free[b]
19	H	18	26	21	176	>500	971/39
37	4-Cl	88	6	9	89	>300	*nd*
38	4-F	34	10	18	127	>300	591/41
39	4-OMe	83	11	17	81	>500	*nd*
40	4-CF_3	72	11	22	210	87	*nd*
41	3-CF_3	40	17	28	>300	>500	5179/155
42	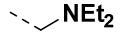	100	<1	<1	3	69	>10.000/-
43	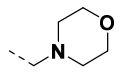	41	<1	<1	5	240	*nd*
44	-	46	6	6	124	51	3200/288
45	-	8	29	47	278	>500	2020/65

[a]Cellular efficacy was determined by measuring prevention of NMDA-induced cleavage of spectrin in rat hippocampal slice cultures. [b]IC_{50} values relating to total and free levels; free levels calculated based on fraction unbound. nd= not determined

P1-Configuration: In general, racemization is an inherent feature of ketoamide-based inhibitors due to the electrophilic group adjacent to the chiral enter. However, although calpain inhibitors have been studied extensively, only Harbeson et al. have reported on studies regarding P1 configuration and the epimerization rates of peptidic calpain inhibitors.[46] In order to determine the potency of the individual enantiomers and to investigate the rate of racemization, we prepared the distinct enantiomers *(S)*- and *(R)*-**19**. Determination of activity *in-vitro* revealed a >500 fold difference in calpain inhibition with the P1 *S*-configuration as the more active enantiomer (K_i Cal 1 (*S*)-**19**= 10 nM).[51] As expected, the distinct enantiomers were configurationally stable in solid form, but underwent pH-dependent racemization in solution. Rapid racemization was observed under physiological conditions at 37°C (assay buffer pH 7.4 or hirudin-anticoagulated rat plasma; calpain inhibition used as read-out), which was completed within two hours *(see Supporting information)*. The individual enantiomers showed a half-life of ~30 min in buffer and 19 min in rat plasma, respectively.

Covalent reversible inhibition: Taking compound **19** as general representative, we studied the dissociation from calpain 1. Assessment of inhibitor off-kinetics by recovery of calpain 1 enzymatic activity after pre-incubation with the inhibitor revealed that that the compound acts as reversible covalent inhibitor of calpain with a half-life $t_{1/2}$= 41 min and a dissociation rate k = 2.85 x 10-4 s^{-1} (*see Supporting Information*).

Addressing potential unspecific reactivity of ketoamide warhead: Overall, we did not find any evidence for unspecific interaction of ketoamide-based calpain inhibitors with cysteine thiols. Inhibition of calpain *in-vitro* was not affected by the presence of glutathione up to 10 mM concentrations. In addition, none of the compounds showed nonspecific reactivity towards the

human La antigen in ALARM NMR, which is a standard in-house assay used to identify thiol reactive compounds.[52]

Selectivity profile: Compounds **19** and **38** did not show cross reactivities for other GPCRs, ion channels and transporters up to 10μM in the CEREP profile (except for the peripheral BZD receptor), and displayed excellent selectivity versus a comprehensive set of different enzymes and proteases including caspases, the proteasome and cathepsins C and H (MDS EnyzmeProfilingScreen at 10μM concentration). Furthermore, none of the compounds displayed any liability against hERG, AMES and micronucleus tests, and rat cardiovascular safety.

Physchemical properties: In terms of physicochemical properties the novel calpain inhibitors are in a chemical space typical for protease inhibitors. Ketoamides **19** and **38** show clogP values of 0.97 and 1.12, respectively, a TPSA of 120, and pass the Lipinski Ro5 and the 3/75 rule.

ADME and PK profile: The *in-vitro* ADME profile for compounds **19** and **38** was characterized by high permeability (P_{app}> 30 x 10^{-6} cm/s) in Caco-2 cells and an efflux ratio of approximately 2. Low aqueous solubility in combination with high permeability puts both compounds in the BCS II class. Plasma protein binding is moderate in both rat and human with approximately 93% bound. Both compounds **19** and **38** had good liver microsomal stability across rat, dog, monkey and human (mClint< 23 μL/min/mg). Hepatocyte stability of **38** was moderate to good in human, monkey, rat and dog (hepClint, μL/min/million cells: 19.4, 13.9, 8.9, and 1.3, respectively). Further metabolite characterization studies using [^{3}H]-labelled **38** revealed significant species differences in its metabolism. In the blood and hepatocytes of human and monkey, **38** is predominantly metabolized by cytosolic carbonyl reductases reducing the ketoamide to the inactive hydroxyamide. In contrast, in rat, **38** is rapidly hydrolyzed in blood to the corresponding keto acid and undergoes oxidation and glucuronidation in hepatocytes. In the

dog, minimal metabolism was observed *in vitro*. Both compounds **19** and **38** demonstrated low potential to elicit clinically significant CYP-mediated drug-drug interactions (DDIs): no direct or time-dependent inhibition of major CYPs and no CYP3A4 mRNA induction was observed. In addition, non-CYP-mediated carbonyl reduction is the primary metabolism pathway.

The pharmacokinetic behaviour of **38** was evaluated in Sprague Dawley rats, Beagle dogs, and Cynomolgus monkeys (**Table 5**). Pharmacokinetics were characterized by high mean plasma clearance (CL_p) in both rat and monkey (CL_p = ~ 2 L/hr•kg), but lower in dog (CL_p = 0.32 L/hr•kg), consistent with *in vitro* hepatocyte stability data. Mean steady state volumes of distribution (V_{ss}) were moderate in all species: 0.65 L/kg in dog and 1.8 L/kg in rat and monkey. The mean elimination half-lives range from 1.1 hours in monkey to 2.9 hours in dog. Oral bio-availability values were moderate to good in dog (F = 30%) and rat (F = 68%), but low in monkey (F =4.5%). Low oral bioavailability and high Cl_p value in monkey are consistent with the ubiquitous distribution of carbonyl reductase activities, the primary metabolizing enzymes for **38**.[53] Compound **38** partitioned into the brain, with brain to plasma drug concentration ratio of ~ 0.2 in rat.

Table 5. Pharmacokinetics of **38** in preclincial species following a single IV or PO dose

	IV					PO					
species	dose	$t_{1/2}$°	$AUC_{0\text{-inf}}$	CL_p	V_{ss}	dose	$t_{1/2}$°	C_{max}	T_{max}	$AUC_{0\text{-inf}}$	F
rat	2	1.7	0.95 (0.13)	2.1 (0.3)	1.8	10	2.6	1.28	0.4 (0.1)	3.22 (0.46)	68 (9.8)
dog	0.5	2.9	1.56 (0.25)	0.3 (0.05)	0.65	1	2.2	0.53	0.3 (0.1)	0.94 (0.50)	30 (15.8)
monkey	1	1.1	0.52 (0.08)	2.0 (0.3)	1.8	10	6.3	0.02	13.3 (10.1)	0.23 (0.032)	4.5 (0.6)

Data provided as mean (standard deviation); ° harmonic mean; Units: Dose (mg/kg); t1/2 (hr); Vss (L/kg); $AUC_{0\text{-inf}}$ (µg•hr/mL); CL_p (L/hr•kg); C_{max} (µg/mL); T_{max} (hr); F (%); IV: intravenous; PO: oral.

Preclinical efficacy: Based on the overall profile compound **38** was selected for extended characterization in a set of AD relevant models. First, we examined the effect of **38** in a panel of *in-vitro* models of neurodegeneration. As already mentioned, compound **38** was shown to prevent neuronal death in rat hippocampal slice cultures via inhibition of NMDA-induced spectrin degradation with an IC_{50} value of 41 nM (Table **4**). In the same system **38** blocked the calpain-mediated proteolysis of intracellular tau with comparable efficacy (IC_{50} of 46 nM free concentration).[54] Application of Aβ globulomer, a specific $A\beta_{1-42}$ oligomer preparation described as neuropathological factor in AD,[55] strongly reduces synaptic transmission in the CA1 area in rat hippocampal slice cultures, and is thus considered as an *in-vitro* model reflecting synaptic degeneration in AD. Co-application of compound **38** (10 nM) completely prevented Aβ globulomer-induced synaptic deficits and restored transmission to a level not significantly different from control (**Figure 5**).

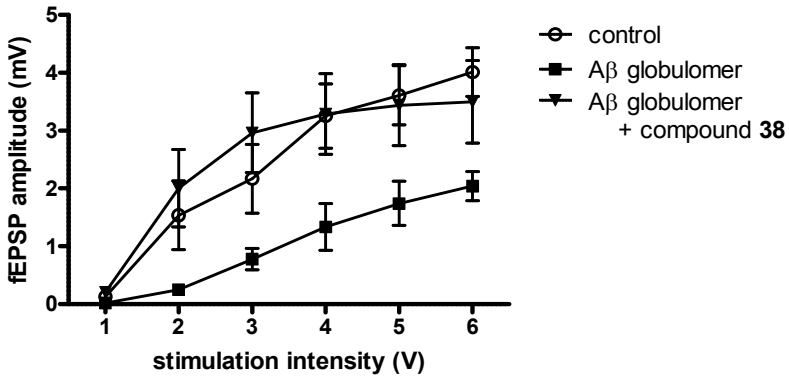

Figure 5 Compound **38** at 10 nM concetration prevents Aβ oligomer-induced deficits in synaptic transmission in rat. Data points are shown as mean +/- SEM. The strength of synaptic transmission is illustrated by the input/output relation in hippocampal slice cultures after stimulation of the Schaffer collateral (p=0.016 when compared to untreated globulomer group; p=0.851 when compared to control).

Since degeneration/dysfunction of cholinergic neurons is closely associated with cognitive deficits in AD, an increase of cholinergic function is widely thought to improve cognitive performance. Inhibitors of acetylcholine-esterase (AChEIs) like donepezil increase extracellular concentration of acetylcholine, thereby i) improving cognition and ii) modifying sleep EEG pattern.[56] We therefore investigated the *in-vivo* effects of **38** on neurotransmission and synaptic function in a microdialysis study. Acute, subcutaneous administration of **38** resulted in a dose-dependent increase in acetylcholine levels in the medial prefrontal cortex reaching significance after administration of 3 and 10 mg/kg, respectively (**Figure 6**), without affecting glutamate and dopamine levels *(data not shown)*.

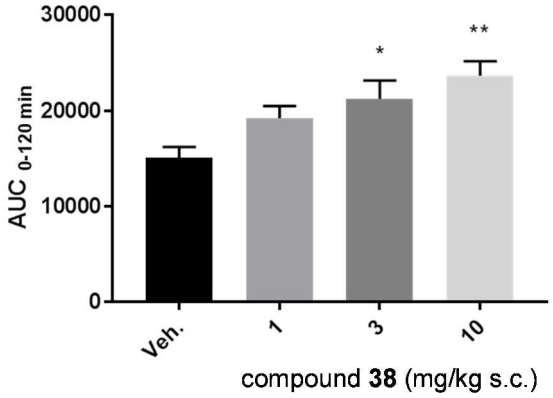

Figure 6 Compound **38** dose-dependently increases microdialysate acetylcholine (ACh) levels in the medial prefrontal cortex. All data are means ± S.E.M. in arbitrary units based on percent change of baseline levels. One-way ANOVA revealed a significant treatment effect for ACh levels [$F(3,41) = 5.82$, $p < 0.0023$]. Subsequent Dunnett´s multiple comparisons demonstrated an increase of ACh levels following administration of **38** at 3 and 10 mg/kg, s.c. (*$p < 0.05$; **$p < 0.01$).

Furthermore, the effects of compound **38** on rat rapid eye movement (REM) sleep pattern were investigated by recording a sleep electroencephalogram (EEG). When given acutely (1-10 mg/kg, p.o.), **38** specifically affected the REM sleep pattern of Fisher rats in a dose-related manner without affecting total sleep (**Table 6**). This is similar to what has been observed with AChEIs such as donepezil *(see Supporting Information)* and suggests that this effect is a functional consequence of increased extracellular ACh.

Table 6. Summary of dose-dependent effects of **38** on rat sleep

Dose (mg/kg)	1	3	10
REM time	105 ± 5	131 ± 6**	125 ± 8**
Latency to REM	100 ± 8	99 ± 10	80 ± 7**
Total sleep time	98 ± 3	105 ± 2	102 ± 2

All parameters are expressed as % of vehicle controls (mean ± SEM) (** $p < 0.01$ from control).

To show that the improvement of cholinergic function translates into enhanced behavioral performance we also explored **38** in a model of cognitive performance in rats. Compound **38** significantly attenuated cognitive impairment induced by the muscarinic antagonist scopolamine in a rat 24 hour passive avoidance paradigm. Administration of scopolamine impaired acquisition of this task, while application of compound **38** (1 mg/kg, s.c. prior to scopolamine) resulted in a significant attenuation of the scopolamine-induced deficits. The dose of 3 mg/kg showed a trend without reaching statistical significance (**Figure 7**).

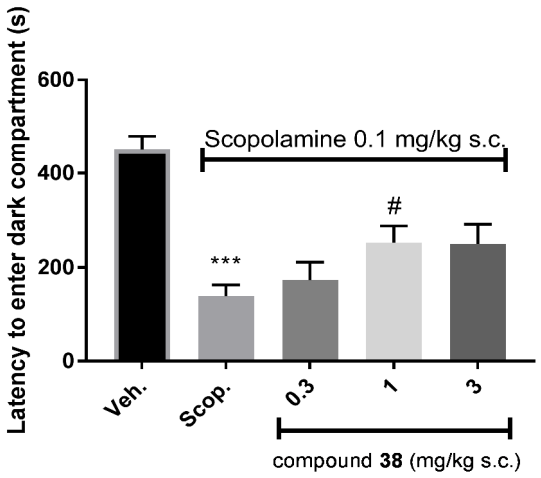

Figure 7. Effect of compound **38** on scopolamine-induced deficits in rats (doses in mg/kg; n=14-47/group). Veh. (vehicle); Scop. (scopolamine, 0.1 mg/kg, s.c.); *** significantly ($p < 0.001$) different from vehicle controls; # ($p < 0.05$) significantly different from scopolamine alone.

Efficacious doses for **38** *in-vivo* were found to be consistent across models with free exposures ranging from approximately 6-25 ng/mL in plasma and 0.2-2.1 ng/g in brain.

In summary, compound **38** showed robust efficacy in various *in-vitro* and *in-vivo* models related to AD. Inhibition of calpain using selective inhibitor **38** resulted in prevention of neurodegeneration and improved neurotransmission, thereby attenuating behavioral deficits. Altogether, these results suggest that novel calpain inhibitors such as **38** have a potential for the treatment of neurodegenerative diseases such as AD.

CONCLUSION

Our goal was to identify novel inhibitors of calpain with enhanced selectivity and favorable PK properties, in particular brain penetration, for the potential treatment of AD. Starting from compound **1** as lead we investigated phenyl-substituted 5-member hetaryls in P3-P2 position in combination with nicotinamide as P2 core. These efforts led to the identification of *N*-(4-amino-3,4-dioxo-1-phenylbutan-2-yl)-2-((3-phenyl-1H-pyrazol-1-yl)nicotinamides as novel series of calpain inhibitors with potencies in the nanomolar range and medium to excellent selectivity versus closely related cysteine protease cathepsins. In particular, compounds **19** and **38** combine favorable cathepsin selectivity, microsomal stability, high cell permeability, and functional efficacy in cellular assays. Potency and enhanced selectivity observed in the 1,3-pyrazole series can be explained via modeling comparing the active sites of calpain 1 and the most relevant cathepsins, respectively. Taking **19** as representative example, we confirmed that potency is dependent on the P1 configuration with the *S*-enantiomer being more active. Due to the adjacent ketoamide the individual enantiomers undergo rapid racemization under *in-vivo* conditions. In addition, **19** was shown to act as covalent reversible inhibitor of calpain, and despite the presence of the ketoamide warhead, no evidence for unspecific reactivity was found. Both compounds were shown to have an excellent profile without liabilities in standard enzyme and receptor panels, DDI, AMES and micronucleus test.

The overall PK profile and brain penetration enabled further advancement of compound **38**. In preclinical models relevant to AD **38** was shown to prevent NMDA-induced neurodegeneration and Aβ-induced synaptic dysfunction. In addition, **38** was shown to enhance neurotransmission which translates into improved cognitive performance. Finally, extended studies in rat and dog such as cardiovascular safety and 14-day tolerability demonstrated an excellent safety

pharmacology profile. Based on the overall favorable results compound **38** was progressed into early clinical development, results will be disclosed in a subsequent publication.[57]

EXPERIMENTAL SECTION

Chemistry: All commercially available chemicals and solvents were used without further purification. In general, reaction mixtures were magnetically stirred at the respective temperature under nitrogen atmosphere. Organic solutions were concentrated under reduced pressure using a Buechi rotovap. Reactions under microwave irradiation conditions were carried out in a Biotage Initiator EXP instrument. Normal phase chromatography was performed on an ISCO CombiFlash Companion MPLC system using RediSep pre-packed columns with silica, reverse phase chromatography was performed using Chromabond C18 cartridges. Reactions were monitored by thin layer chromatography using HPTLC Silicagel 60 F254 plates from Merck KGaA, and were visualized using 254 nm ultraviolet light and/or exposure to silica gel impregnated with iodine. Optical rotations were obtained on a PerkinElmer polarimeter 341. All new compounds gave satisfactory ^{1}HNMR and LC/MS. On the basis of LCMS, all final compounds were >95% pure unless otherwise noted. NMR spectra were obtained on a Bruker Avance I 400 MHz, Avance III 500 MHz or 600 MHz NMR spectrometer using residual signal of deuterated NMR solvent as internal reference; chemical shifts for protons are reported in a parts per million scale downfield from tetramethylsilane. Analytical LCMS data were obtained using an Agilent 1100 series HPLC system with DAD and SQ mass spectrometer with ESI in positive mode and a scan range of 100-700 amu. Samples were run on a Chromasil 80 ODS-7pH column 4µm, 40x2mm; gradient elution 5-100% B over 10 minutes; solvent A: H2O/0.1% TFA; solvent B: acetonitrile/0.1% TFA; flow rate: 0.5 mL/min; temperature: 60°C. Chiral compounds

were analyzed by chiral HPLC using an Agilent 1100 HPLC with samples run on Chiralpak AD-H 4.6mmID x 250 mm; 5μ; with n-hexane/EtOH/MeOH 20/40/40 as mobile phase; flow rate: 0.6 /min and detection at 300nm wavelength. Chemical names were generated using ChemDraw Professional 15.0 (Perkin-Elmer Informatics). Modeling studies were performed using InsightII from Accelrys/MSI.

***N*-(4-(1*H*-Pyrazol-3-yl)benzyl)-N-ethylethanamine** (**8a**). A mixture of 1-(4-((diethylamino)-methyl)phenyl)ethan-1-one (11.9 g, 57.96 mmol) and DMF dimethylacetal (7.6 g, 57.96 mmol) was heated in a microwave to 200°C for 20 minutes. After cooling to rt first EtOH (200 mL) and then hydrazine hydrate (10.3 g, 316.1 mmol - dropwise) were added and the reaction heated to reflux for 2 hours. Afterwards the mixture was concentrated, HCl (1 M in water) added to adjust pH~1 and extracted twice with MTBE. The aqueous layer was basified with NaOH (1 M in water), the product extracted into MTBE (x2), and the combined organic extracts were dried (Na_2SO_4) and concentrated to give a pale yellow oil (13.3 g, 91.7%) which was used in the next reaction without further purification. ^{1}H NMR (400 MHz, DMSO-d_6 – mixture of tautomers) δ 13.22 and 12.80 (s, 1H), 7.80–7.60 (m, 3H), 7.32 (d, J = 7.9 Hz, 2H), 6.65 (d, J = 8.6 Hz, 1H), 3.52 (s, 2H), 2.50 – 2.36 (q, overlap with DMSO, 2 H), 0.98 (t, J = 7.1 Hz, 3H). ESI MS (m/z): calcd for $C_{14}H_{19}N_3$, 229.2; found 230.1 [M + H^+].

4-(4-(1*H*-Pyrazol-3-yl)benzyl)morpholine (**8b**). 1-(4-(Morpholinomethyl)phenyl)ethan-1-one (10.5g, 47.9 mmol) was converted into the pyrazole in analogy to the preparation of **8a** giving the title compound as pale yellow oil (12.3 g, 97%). ^{1}H NMR (400 MHz, DMSO-d_6, mixture of tautomers) δ 13.24 and 12.82 (s, 1H), 7.80–7.58 (m, 3H), 7.323 (d, J = 7.8 Hz, 2H), 6.66 (d, J = 7.5 Hz, 1H), 3.57 (m, 4H), 3.46 (s, 2H), 2.36 (m, 4H). ESI MS (m/z): calcd for $C_{14}H_{17}N_3O$, 243.1; found 244.1 [M + H^+].

Methyl 2-(2-phenylthiazol-4-yl)nicotinate (9). $PyBr_3$ (4.5 g, 14.07 mmol) – suspended in acetic acid (15 mL) – was added to a solution of methyl 2-acetylnicotinate (2.4 g, 13.39 mmol) in hydrogen bromide (33% solution in acetic acid, 6 mL), and stirred for 3 hours at rt. The mixture was filtered, the precipitate obtained washed with n-pentane and then dried to give 3.45 g (68.4%) of the bromide as off-white solid, which was used in the next step without further purification. The mixture of 2-(2-bromoacetyl)-3-(methoxycarbonyl)pyridinium bromide (1.15 g, 3.05 mmol) and benzothioamide (0.5 g, 3.64 mmol) in DMF (12 mL) was stirred for 1 hr at rt and then concentrated to give a brownish oil. Purification by chromatography (silica gel, dichloromethane/MeOH as eluent) gave thiazole **9** as a pale yellow oil (0.8 g, 88%). ^{1}H NMR (400 MHz, DMSO-d_6) δ 8.77 (dd, J = 4.9, 1.7 Hz, 1H), 8.37 (s, 1H), 8.02 (dd, J = 7.8, 1.7 Hz, 1H), 7.99–7.88 (m, 2H), 7.62–7.37 (m, 4H), 3.75 (s, 3H). ESI MS (m/z): calcd for $C_{16}H_{12}N_2O_2S$, 296.1; found 297.1 [$M + H^+$].

2-(2-Phenylthiazol-4-yl)nicotinic acid (10). NaOH (2 M in water, 4 mL) was added dropwise to a solution of methyl 2-(2-phenylthiazol-4-yl)nicotinate **9** (0.62 g, 2.1 mmol) in MeOH (15 mL), and the mixture heated for 1 hr to 70°C. The mixture then was concentrated, the obtained residue dissolved in water, acidified to pH5 using 2 M HCl (4 mL), the precipitate collected, washed twice with water and dried to give **10** as off-white solid (0.35 g, 59.3%). ^{1}H NMR (400 MHz, DMSO-d_6) δ 13.14 (s, 1H), 8.72 (d, J = 4.6 Hz, 1H), 8.28 (s, 1H), 8.04–7.95 (m, 3H), 7.58–7.45 (m, 4H). ESI MS (m/z): calcd for $C_{15}H_{10}N_2O_2S$, 282.1; found 283.0 [$M + H^+$].

Ethyl 2-(4-phenylthiazol-2-yl)nicotinate (11). Reaction of ethyl 2-carbamoylnicotinate (2.8 g, 10.65 mmol) and 2-bromo-1-phenlyethanone (2.3 g, 11.56 mmol) in DMF (35 mL) in analogy to **9** and purification by chromatography gave thiazole **11** as off-white solid (2.79 g, 84%). ^{1}H NMR (400 MHz, DMSO-d_6) δ 8.77 (dd, J = 4.8, 1.6 Hz, 1H), 8.33 (s, 1H), 8.07 (dd, J = 7.8, 1.7

Hz, 1H), 8.02–7.93 (m, 2H), 7.63 (dd, J = 7.8, 4.8 Hz, 1H), 7.49 (dd, J = 8.3, 6.9 Hz, 2H), 7.43–7.34 (m, 1H), 4.35 (q, J = 7.1 Hz, 2H), 1.15 (t, J = 7.1 Hz, 3H). ESI MS (m/z): calcd for $C_{17}H_{14}N_2O_2S$, 310.1; found 311.1 [M + H^+].

2-(4-Phenylthiazol-2-yl)nicotinic acid (12). Hydrolysis of ethyl 2-(4-phenylthiazol-2-yl)nicotinate **11** (1.88 g, 6.06 mmol) in analogy to **10** gave compound **12** as off-white solid (1.5 g, 88%). ^{1}H NMR (400 MHz, DMSO-d_6) δ 13.43 (s, 1H), 8.73 (dd, J = 4.6, 1.5 Hz, 1H), 8.30 (s, 1H), 8.03 (m, 3H), 7.59 (dd, J = 7.7, 4.8 Hz, 1H), 7.48 (m, 2H), 7.39 (m, 1H). ESI MS (m/z): calcd for $C_{15}H_{10}N_2O_2S$, 282.0; found 283.1 [M + H^+].

Ethyl 2-(2-phenyloxazol-4-yl)nicotinate (13). PEPPSI-IPr (22.0 mg, 0.032 mmol) was added to a mixture of ethyl-2-chloronicotinate (120.0 mg, 0.647 mmol) and 2-phenyl-4-(4,4,5,5-tetramethyl-1,3,2-dioxaborolan-2-yl)oxazole (220 mg, 0.811 mmol) in dioxane (5 mL). K_2CO_3 (402.0 mg, 2.91 mmol) was added and the reaction mixture was heated for 4 hours at 65°C. After cooling to rt water was added and the mixture was extracted with EtOAc. The combined organic layers were washed with water, dried ($MgSO_4$) and concentrated. Purification by chromatography (silica gel, gradient 5-10% EtOAc in dichloromethane) gave compound **13** as oil (80 mg, 42.0%). ^{1}H NMR (500 MHz, DMSO-d_6) δ 8.77–8.71 (m, 2H), 8.05–7.97 (m, 3H), 7.61–7.56 (m, 3H), 7.51 (dd, J = 7.9, 4.8 Hz, 1H), 4.32 (q, J = 7.1 Hz, 2H), 1.16 (t, J = 7.1 Hz, 3H). ESI MS (m/z): calcd for $C_{17}H_{14}N_2O_2$, 294.1; found 295.1 [M + H^+].

2-(2-Phenyloxazol-4-yl)nicotinic acid (14). NaOH (0.27 mL, 2M in water, 0.544 mmol) was added to a solution of ethyl 2-(2-phenyloxazol-4-yl)nicotinate **13** (80.0 mg, 0.272 mmol) in EtOH (2.7 mL). After stirring overnight the mixture was concentrated in vacuo. The residue obtained was dissolved in water and HCl (2 M in water) was added to adjust the pH to ~1. The

solvent was removed in vacuo to give a solid residue, which was used without further purification (120 mg). ESI MS (m/z): calcd for $C_{15}H_{10}N_2O3$, 266.1; found 267.1 [M + H^+].

Benzyl ((2*S*,3*R*)-4-amino-3-hydroxy-4-oxo-1-phenylbutan-2-yl)carbamate (**15a**). DMSO (3.45 mL, 48.6 mmol) in dichloromethane (10 mL) was added dropwise to a solution of oxalylchloride (1.85 mL, 21.57 mmol) in dichloromethane (70 mL)) at -70° C. After allowing the reaction to stir for 10 minutes, a solution of benzyl (*S*)-(1-hydroxy-3-phenylpropan-2-yl)carbamate (5.3 g, 18.57 mmol) in a mixture of dichloromethane (30 mL) and DMSO (0.5 mL) and then triethylamine (6 mL) was added dropwise. The mixture was kept for 1 hour at -70°C, then a solution of trimethylsilylcyanide (2.05 g, 20.7 mmol) in dichloromethane (10 mL) was added under the same conditions, the reaction kept at -70°C for 4 hours and the temperature then allowed to slowly rise to rt overnight. Water (50 mL) was added, the organic layer washed again, dried (Na_2SO_4) and concentrated. The solid obtained was dissolved in THF (60 mL), cooled to 10°C, acidified by dropwise addition of 1 N HCl (7 mL) and stirred for 30 minutes at rt. Brine (70 mL) and diethylether (70 mL) were added, the organic layer dried (Na_2SO_4) and concentrated. The remaining yellow oil (8.8 g) was treated with diisopropylether for 2 hours, the precipitate formed was collected and dried to give benzyl ((1*R*,2*S*)-1-cyano-1-hydroxy-3-phenylpropan-2-yl)carbamate as an off-white solid (3.5 g, 60.7%). $[\alpha]^{20}_D$ = -81.8 (1% in DMF). ^{1}H NMR (400 MHz, Chloroform-*d*) δ 7.42–7.23 (m, 9H), 7.22–7.13 (m, 2H), 5.28–4.96 (m, 3H), 4.57 (s, 1H), 3.99 (m, 1H), 3.13 (dd, J = 14.4, 6.4 Hz, 1H), 2.96 (dd, J = 14.1, 8.5 Hz, 1H).

To a solution of benzyl ((1*R*,2*S*)-1-cyano-1-hydroxy-3-phenylpropan-2-yl)carbamate (5.4 g, 17.4 mmol) in dioxane (100 mL) conc. HCl (100 mL) was added dropwise at 10°C and the reaction then allowed to stir overnight at rt. The mixture was poured into water (1000 mL) and extracted with EtOAc (3 x 300mL), the combined organic layers dried (Na_2SO_4) and

concentrated. The residue obtained was treated with diisopropylether, the solid collected and dried to give a **15a** as a white amorphous solid (4.26 g, 74.5%). $[\alpha]^{20}_{D}$= -36.2 (1% in DMF).). ESI MS (m/z): calcd for $C_{18}H_{20}N_2O_4$, 328.1; found 329.1 [M + H^+].

(2*R*,3*S*)-3-Amino-2-hydroxy-4-phenylbutanamide (16a). Compound **15a** (2.48g, 7.55 mmol) was hydrogenated over 10% Pd/C (0.15 g) in a mixture of MeOH (80 mL) and 2 N HCl (4.2 mL). The reaction mixture was filtered over Celite and concentrated. The obtained solid then was treated with n-pentane (100 mL) to give **16a** as an amorphous white solid (1.66 g, 95.3%). ^{1}H NMR (600 MHz, Methanol-d_4) δ 7.44–7.21 (m, 5H), 4.03 (d, J = 2.3 Hz, 1H), 3.81 (ddd, J = 8.8, 6.6, 2.3 Hz, 1H), 3.07 (dd, J = 13.8, 8.7 Hz, 1H), 2.96 (dd, J = 13.7, 6.6 Hz, 1H). ESI MS (m/z): calcd for $C_{10}H_{14}N_2O_2$, 194.1; found 195.05 [M + H^+].

(2*S*,3*R*)-3-Amino-2-hydroxy-4-phenylbutanamide x HCl (16b). Synthesis of **16b** was carried out in analogy to the preparation described for **16a** starting from benzyl (*R*)-(1-hydroxy-3-phenylpropan-2-yl)carbamate giving benzyl (2*S*,3*R*)-4-amino-3-hydroxy-4-oxo-1-phenyl¬butan-2-yl)carbamate **15b** (1.9 g, 56.1%). $[\alpha]^{20}_{D}$= +37.8 (1% in DMF). Hydrogenolytic cleavage of the benzyloxycarbonyl group gave **16b** (1.2 g, 96.4%). ^{1}H NMR (600 MHz, Methanol-*d4*) δ 7.48–7.14 (m, 5H), 4.02 (d, J = 2.3 Hz, 1H), 3.81 (ddd, J = 8.8, 6.7, 2.3 Hz, 1H), 3.07 (dd, J = 13.8, 8.7 Hz, 1H), 2.96 (dd, J = 13.8, 6.6 Hz, 1H).

*Representative procedure: Synthesis of N-(4-amino-3,4-dioxo-1-phenylbutan-2-yl)-2-(3-phenyl-1H-pyrazol-1-yl)nicotinamide (**19**)*

Ethyl 2-(3-phenyl-1*H*-pyrazol-1-yl)nicotinate (5). To the solution of 3-phenyl-1*H*-pyrazole (4.3 g, 29.82 mmol) and ethyl 2-chloronicotinate (11.63 g, 62.63 mmol) in DMF (50 mL) 18-crown-6 (0.07 g), K_2CO_3 (7.17 g) and KI (0.29 g) were added and the mixture was heated at 130°C. After completion of the reaction water was added, extracted with EtOAc, the organic

layer washed with water and brine, dried (Na_2SO_4) and concentrated. Purification by chromatography (silica gel, dichloromethane as eluent) gave compound **5** as colorless oil (7.5 g, 85.1%). ^{1}H NMR (400 MHz, DMSO-d_6) δ 8.63 (dd, J = 4.9, 1.7 Hz, 1H), 8.58 (d, J = 2.7 Hz, 1H), 8.13 (dd, J = 7.6, 1.7 Hz, 1H), 7.90–7.82 (m, 2H), 7.56–7.44 (m, 3H), 7.42–7.32 (m, 1H), 7.10 (d, J = 2.7 Hz, 1H, 4.23 (d, J = 7.1 Hz, 2H), 1.08 (t, J = 7.1 Hz, 3H). ESI MS (m/z): calcd for $C_{17}H_{15}N_3O_2$, 293.1; found 294.1 [M + H$^+$].

2-(3-Phenyl-1*H*-pyrazol-1-yl)nicotinic acid (**6**). NaOH (2 M in water, 28 mL) was added dropwise to a solution of **5** (7.0 g, 23.86 mmol) in MeOH (100 mL) and the reaction stirred overnight at rt. The mixture then was concentrated, diluted with water (100 mL) and brought to pH 6 by addition of 2 M HCl (30 mL). After extraction with dichloromethane the organic layer was washed with brine, dried (Na_2SO_4) and concentrated. The remaining oil was taken up in MTBE (15 mL), upon addition of n-pentane (50 mL) a white precipitate formed which was collected and dried to give **6** as a white solid (5.8 g, 91.6%). ^{1}H NMR (400 MHz, DMSO-d_6) δ 8.59 (dd, J = 4.9, 1.8 Hz, 1H), 8.55 (d, J = 2.7 Hz, 1H), 8.09 (dd, J = 7.6, 1.8 Hz, 1H), 7.91 (d, J = 7.5 Hz, 2H), 7.47 (dt, J = 10.0, 6.3 Hz, 3H), 7.38 (t, J = 7.3 Hz, 1H), 7.07 (d, J = 2.7 Hz, 1H).). ESI MS (m/z): calcd for $C_{15}H_{11}N_3O_2$, 265.1; found 266.1 [M + H$^+$].

***N*-(4-Amino-3-hydroxy-4-oxo-1-phenylbutan-2-yl)-2-(3-phenyl-1*H*-pyrazol-1-yl)nicotinamide** (**7**). To a solution of **6** (6.0 g, 30.17 mmol) in dichloromethane (200 mL) at 5°C were added subsequently EDCI (5.4g, 28.17 mmol), HOBt (3.8g, 28.12 mmol) and trimethylamine (4.2 mL, 30.17 mmol). After 30 minutes of stirring 3-amino-2-hydroxy-4-phenylbutanamide (4.5 g, 23.17 mmol) was added and after 5 minutes pH 10 re-adjusted by addition of triethylamine (0.4 mL). The mixture was then stirred for another hour at 5°C, and then overnight at rt. Concentration and treatment of the residue with water (300 mL) gave a

solid, which was collected and dried (9.6 g). Recristallization from EtOH (300 mL) yielded **7** as a white amorphous solid (8.7g, 85%). ESI MS (m/z): calcd for $C_{25}H_{23}N_5O_3$, 441.2; found 442.1 [M + H+].

***N*-(4-Amino-3,4-dioxo-1-phenylbutan-2-yl)-2-(3-phenyl-1*H*-pyrazol-1-yl)nicotinamide** (**19**). To a solution of **7** (6.21 g, 14.0 mmol) in DMSO (100 mL) EDCI (20.8 g, 108.5 mmol) was added in several portions and the mixture stirred for about 30 minutes. Dichloroacetic acid (8.07 g, 62.1 mmol) was added dropwise over 15 minutes under cooling with ice water bath, and the reaction allowed to stir for another hour. The mixture then was poured into water (800 mL), and after stirring for 20 minutes the precipitate formed was collected, washed with water and dried. The obtained crude product (mixture of ketoamide and corresponding hydrate) was suspended in MeOH (500 mL), HCl (4 M in dioxane, 4 mL) added and the resulting clear solution concentrated again. The solid obtained was digested subsequently with EtOAc (100 mL) and n-pentane (200 mL), the remaining solid collected and dried to give the title compound as a white solid (3.7 g, 60.2%). ^{1}H NMR (500 MHz, DMSO-d_6) δ 8.95 (d, J = 7.0 Hz, 1H), 8.55 (dd, J = 4.7, 1.8 Hz, 1H), 8.47 (d, J = 2.7 Hz, 1H), 8.07 (s, 1H), 7.85 (s, 1H), 7.80–7.74 (m, 2H), 7.72 (dd, J = 7.6, 1.8 Hz, 1H), 7.46 (dd, J = 7.6, 4.8 Hz, 1H), 7.39 (dd, J = 8.2, 6.5 Hz, 2H), 7.36–7.29 (m, 1H), 7.22–7.11 (m, 5H), 7.00 (d, J = 2.7 Hz, 1H), 5.71–5.37 (m, 1H), 3.14 (dd, J = 14.2, 4.7 Hz, 1H), 2.79 (dd, J = 14.1, 8.9 Hz, 1H). ^{13}C NMR (126 MHz, DMSO-d_6) δ 196.93, 166.98, 162.84, 152.85, 149.22, 147.44, 139.38, 137.55, 132.83, 130.44, 129.34, 129.07, 128.62, 126.90, 125.90, 124.45, 122.22, 105.69, 55.32, 36.07. ESI MS (m/z): calcd for $C_{25}H_{21}N_5O_3$, 439.2; found 440.2 [M + H^+].

(*S*)-*N*-(4-Amino-3,4-dioxo-1-phenylbutan-2-yl)-2-(3-phenyl-1H-pyrazol-1-yl)nicotinamide (*S*)-19. Analogous synthesis using (2*R*,3*S*)-3-amino-2-hydroxy-4-phenylbutanamide (**16a**) as

starting material gave (*S*)-**19** as a white solid (0.35 g, 50.2%). $[\alpha]^{20}_{D}$= +71.0 (1% in DMF). Chiral HPLC Rt: 13.28 min; 94% ee.

(*R*)-*N*-(4-Amino-3,4-dioxo-1-phenylbutan-2-yl)-2-(3-phenyl-1*H*-pyrazol-1-yl)nicotinamide (*R*)-19. Analogous synthesis using (2*S*,3*R*)-3-amino-2-hydroxy-4-phenylbutanamide (**16b**) as starting material gave (*R*)-**16** as a white solid (0.25g, 66%). $[\alpha]^{20}_{D}$= -62.1 (1% in DMF). Chiral HPLC Rt: 28.47 min; 90% ee.

Compound 17, 18 and 20-45. Compounds were synthesized in a similar manner as described for **19** using the appropriate starting materials; detailed descriptions are given in the literature.[58-60]

***N*-(4-Amino-3,4-dioxo-1-phenylbutan-2-yl)-2-(4-phenyl-1*H*-imidazol-1-yl)nicotinamide** (**17**). (8.7%) ^{1}H NMR (500 MHz, DMSO-d_6) δ 9.50 (d, J = 7.5 Hz, 1H), 8.76–8.66 (m, 2H), 8.15 (s, 1H), 8.11 (d, J = 1.5 Hz, 1H), 7.99–7.80 (m, 4H), 7.68 (dd, J = 7.7, 4.9 Hz, 1H), 7.47 (m, 2H), 7.36 (m, 1H), 7.26 (m, 4H), 7.18 (d, J = 4.7 Hz, 1H), 5.42 (m, 1H), 3.22 (dd, J = 14.0, 4.0 Hz, 1H), 2.85 (dd, J = 14.0, 9.9 Hz, 1H). ESI MS (m/z): calcd for $C_{25}H_{21}N_5O_3$, 439.2; found 440.3 [M + H$^+$].

***N*-(4-Amino-3,4-dioxo-1-phenylbutan-2-yl)-2-(4-phenyl-1*H*-pyrazol-1-yl)nicotinamide (18)**. (91%) ^{1}H NMR (500 MHz, DMSO-d_6) δ 8.91 (d, J = 7.2 Hz, 1H), 8.85 (s, 1H), 8.56 (dd, J = 4.8, 1.8 Hz, 1H), 8.04 (s, 2H), 7.80 (s, 1H), 7.77–7.68 (m, 3H), 7.47 (dd, J = 7.6, 4.8 Hz, 1H), 7.41 (m, 2H), 7.33–7.22 (m, 4H), 7.19 (m, 1H), 5.49–5.23 (m, 1H), 3.16 (dd, J = 14.3, 4.3 Hz, 1H), 2.89 (dd, J = 14.3, 9.2 Hz, 1H). ESI MS (m/z): calcd for $C_{25}H_{21}N_5O_3$, 439.2; found 440.1 [M + H$^+$].

***N*-(4-Amino-3,4-dioxo-1-phenylbutan-2-yl)-2-(2-phenylthiazol-4-yl)nicotinamide (20).** (74.9%) ^{1}H NMR (400 MHz, DMSO-d_6) δ 8.83 (d, J = 6.9 Hz, 1H), 8.68 (dd, J = 4.7, 1.8 Hz,

1H), 8.09 (s, 1H), 8.02 (s, 1H), 7.88–7.78 (m, 3H), 7.62 (dd, J = 7.8, 1.8 Hz, 1H), 7.50–7.40 (m, 4H), 7.16 (d, J = 4.5 Hz, 5H), 5.55 (m, 1H), 3.12 (dd, J = 14.1, 4.4 Hz, 1H), 2.75 (dd, J = 14.1, 9.3 Hz, 1H). ESI MS (m/z): calcd for $C_{25}H_{20}N_4O_3S$, 456.1; found 457.1 [M + H^+].

***N*-(4-Amino-3,4-dioxo-1-phenylbutan-2-yl)-2-(2-phenyloxazol-4-yl)nicotinamide (21).** (51.5%) ^{1}H NMR (400 MHz, DMSO-d_6) δ 8.98 (d, J = 7.1 Hz, 1H), 8.68 (dd, J = 4.7, 1.8 Hz, 1H), 8.40 (s, 1H), 8.07 (s, 1H), 7.91 (dd, J = 6.7, 2.9 Hz, 2H), 7.84 (s, 1H), 7.62 (dd, J = 7.6, 1.7 Hz, 1H), 7.54 (dd, J = 5.2, 2.0 Hz, 3H), 7.46 (dd, J = 7.7, 4.7 Hz, 1H), 7.34–6.98 (m, 5H), 5.52 (m, 1H), 3.18 (dd, J = 14.0, 4.2 Hz, 1H), 2.81 (dd, J = 14.1, 9.6 Hz, 1H). ESI MS (m/z): calcd for $C_{25}H_{20}N_4O_4$, 440.1; found 441.1 [M + H^+].

***N*-(4-Amino-3,4-dioxo-1-phenylbutan-2-yl)-2-(4-phenylthiazol-2-yl)nicotinamide (22).** (61.5%) ^{1}H NMR (400 MHz, DMSO-d_6) δ 8.93 (d, J = 6.9 Hz, 1H), 8.69 (d, J = 4.7 Hz, 1H), 8.22 (s, 1H), 8.02 (s, 1H), 7.88 (d, J = 7.5 Hz, 2H), 7.81 (s, 1H), 7.60 (m, 2H), 7.48–7.23 (m, 3H), 7.23–6.87 (m, 5H), 5.69 (m, 1H), 3.15 (dd, J = 14.2, 4.6 Hz, 1H), 2.91–2.68 (m, 1H). ESI MS (m/z): calcd for $C_{25}H_{20}N_4O_8S$, 456.1; found 457.2 [M + H^+].

***N*-(4-Amino-3,4-dioxo-1-phenylbutan-2-yl)-2-(3-phenyl-1*H*-pyrazol-1-yl)benzamide (23).** (26.3%) ^{1}H NMR (400 MHz, DMSO-d_6) δ 9.01 (d, J = 7.4 Hz, 1H), 8.07 (s, 1H), 7.82 (d, J = 8.1 Hz, 3H), 7.75–7.68 (m, 2H), 7.64–7.56 (m, 1H), 7.42 (m, 3H), 7.38–7.18 (m, 7H), 6.81 (d, J = 2.5 Hz, 1H), 5.52–5.25 (m, 1H), 3.20 (dd, J = 13.8, 4.6 Hz, 1H), 2.78 (dd, J = 14.0, 9.9 Hz, 1H). ESI MS (m/z): calcd for $C_{26}H_{22}N_4O_3$, 438.2; found 439.1 [M + H^+].

***N*-(4-Amino-3,4-dioxo-1-phenylbutan-2-yl)-2-(2-phenylthiazol-4-yl)benzamide (24).** (35.5%) ^{1}H NMR (400 MHz, DMSO-d_6) δ 8.90 (d, J = 7.5 Hz, 1H), 8.09 (s, 1H), 7.98–7.86 (m, 3H), 7.84 (s, 1H), 7.60–7.47 (m, 4H), 7.44 (m, 1H), 7.35 (s, 1H), 7.26 (m, 5H), 5.45 (m, 1H),

3.19 (dd, J = 13.9, 3.9 Hz, 1H), 2.78 (dd, J = 13.9, 10.1 Hz, 1H). ESI MS (m/z): calcd for $C_{26}H_{21}N3O_3S$, 455.1; found 456.1 [M + H^+].

***N*-(1-Amino-1,2-dioxoheptan-3-yl)-2-(4-phenyl-1H-imidazol-1-yl)nicotinamide (25)**. (18.6%) ^{1}H NMR (400 MHz, DMSO-d_6) δ 9.15 (d, J = 7.0 Hz, 1H), 8.66 (dd, J = 4.8, 1.8 Hz, 1H), 8.12 (d, J = 1.3 Hz, 1H), 8.07 (s, 1H), 8.01 (dd, J = 7.7, 1.8 Hz, 1H), 7.95 (d, J = 1.3 Hz, 1H), 7.84–7.80 m, 3H), 7.58 (dd, J = 7.7, 4.9 Hz, 1H), 7.39 (t, J = 7.7 Hz, 2H), 7.25 (m, 1H), 5.15 (m, 1H), 1.75 (m, 1H), 1.50 (m, 1H), 1.37–1.11 (m, 4H), 0.77 (t, J = 6.9 Hz, 3H). ESI MS (m/z): calcd for $C_{22}H_{23}N_5O_3$, 405.2; found 406.2 [M + H^+].

***N*-(1-Amino-1,2-dioxoheptan-3-yl)-2-(4-phenyl-1*H*-pyrazol-1-yl)nicotinamide (26).** (77.9%) ^{1}H NMR (500 MHz, DMSO-d_6) δ 8.86 (s, 1H), 8.67 (d, J = 6.9 Hz, 1H), 8.59 (dd, J = 4.9, 1.8 Hz, 1H), 8.14 (s, 1H), 8.00 (s, 1H), 7.86 (dd, J = 7.6, 1.9 Hz, 1H), 7.79–7.66 (m, 3H), 7.50 (dd, J = 7.5, 4.8 Hz, 1H), 7.40 (t, J = 7.6 Hz, 2H), 7.26 (t, J = 7.4 Hz, 1H), 5.09 (m, 1H), 1.83–1.67 (m, 1H), 1.56–1.41 (m, 1H), 1.39–1.10 (m, 4H), 0.81 (t, J = 6.7 Hz, 3H). ESI MS (m/z): calcd for $C_{22}H_{23}N_5O_3$, 405.2; found 406.2 [M + H^+].

***N*-(1-Amino-1,2-dioxoheptan-3-yl)-2-(3-phenyl-1*H*-pyrazol-1-yl)nicotinamide (27)**. (39.4%) ^{1}H NMR (400 MHz, DMSO-d_6) δ 8.72 (d, J = 6.6 Hz, 1H), 8.57 (dd, J = 4.9, 1.7 Hz, 1H), 8.50 (d, J = 2.6 Hz, 1H), 8.01 (s, 1H), 7.86 (m, 3H), 7.77 (s, 1H), 7.49 (dd, J = 7.6, 4.8 Hz, 1H), 7.43 (t, J = 7.4 Hz, 2H), 7.36 (m, 1H), 7.03 (d, J = 2.5 Hz, 1H), 5.15 (m, 1H), 1.69 (m, 1H), 1.43 (m, 1H), 1.28–0.98 (m, 4H), 0.67 (t, J = 6.9 Hz, 3H). ESI MS (m/z): calcd for $C_{22}H_{23}N_5O_3$, 405.2; found 406.1 [M + H^+].

***N*-(1-Amino-1,2-dioxoheptan-3-yl)-2-(2-phenylthiazol-4-yl)nicotinamide (28)**. (48.7%) ^{1}H NMR (400 MHz, DMSO-d_6) δ 8.70 (dd, J = 4.8, 1.7 Hz, 1H), 8.65 (d, J = 6.6 Hz, 1H), 8.22 (s, 1H), 7.97 (s, 1H), 7.94 m, 2H), 7.78 (dd, J = 7.8, 1.7 Hz, 1H), 7.74 (s, 1H), 7.50 (m, 4H), 5.15

(m, 1H), 1.67 (m, 1H), 1.41 (m, 1H), 1.11 (m, 4H), 0.67 (m, 3H). ESI MS (m/z): calcd for $C_{22}H_{22}N_4O_3S$, 422.1; found 423.1 [M + H^+].

***N*-(4-Amino-3,4-dioxo-1-phenylbutan-2-yl)-2-(1H-pyrazol-1-yl)nicotinamide (29)**. (60.9%) 1H NMR (600 MHz, DMSO-d_6) δ 8.92 (d, J = 7.1 Hz, 1H), 8.59–8.46 (m, 1H), 8.39 (d, J = 2.6 Hz, 1H), 8.08 (s, 1H), 7.83 (s, 1H), 7.77–7.63 (m, 1H), 7.58 (s, 1H), 7.45 (dd, J = 7.6, 4.8 Hz, 1H), 7.36–7.16 (m, 5H), 5.35 (m, 1H), 3.14 (dd, J = 14.4, 4.3 Hz, 1H), 2.86 (dd, J = 14.4, 9.3 Hz, 1H). ESI MS (m/z): calcd for $C_{19}H_{17}N_5O_3$, 363.1; found 364.1 [M + H^+].

***N*-(4-Amino-3,4-dioxo-1-phenylbutan-2-yl)-2-(3-cyclohexyl-1*H*-pyrazol-1-yl)nicotinamide (30)**. (67.5%). ^{1}H NMR (400 MHz, DMSO-d_6) δ 8.81 (d, J = 6.8 Hz, 1H), 8.49 (dd, J = 4.8, 1.7 Hz, 1H), 8.27 (d, J = 2.5 Hz, 1H), 8.04 (s, 1H), 7.81 (s, 1H), 7.67 (dd, J = 7.6, 1.7 Hz, 1H), 7.39 (dd, J = 7.5, 4.8 Hz, 1H), 7.32–7.20 (m, 5H), 6.32 (d, J = 2.4 Hz, 1H), 5.44 (m, 1H), 3.14 (dd, J = 14.1, 4.8 Hz, 1H), 2.86 (dd, J = 14.0, 8.5 Hz, 1H), 2.44 (m, overlapping with DMSO), 1.94–1.51 (m, 6H), 1.24 (q, J = 12.8, 11.5 Hz, 4H). ESI MS (m/z): calcd for $C_{25}H_{27}N_5O_3$, 445.2; found 446.2 [M + H^+].

***N*-(4-Amino-3,4-dioxo-1-phenylbutan-2-yl)-2-(3-(tert-butyl)-1*H*-pyrazol-1-yl)nicotinamide (31)**. (93%). ^{1}H NMR (400 MHz, DMSO-d_6) δ 8.82 (d, J = 6.6 Hz, 1H), 8.49 (d, J = 4.7 Hz, 1H), 8.25 (d, J = 2.5 Hz, 1H), 8.05 (s, 1H), 7.81 (s, 1H), 7.68 (d, J = 7.5 Hz, 1H), 7.40 (dd, J = 7.6, 4.8 Hz, 1H), 7.25 (m, 5H), 6.37 (d, J = 2.6 Hz, 1H), 5.52–5.42 (m, 1H), 3.14 (dd, J = 13.8, 4.6 Hz, 1H), 2.81 (dd, J = 14.0, 8.8 Hz, 1H), 1.12 (s, 9H). ESI MS (m/z): calcd for $C_{23}H_{25}N_5O_3$, 419.2; found 420.2 [M + H^+].

***N*-(4-Amino-3,4-dioxo-1-phenylbutan-2-yl)-2-(3-cyclopropyl-1*H*-pyrazol-1-yl)nicotinamide (32)**. ^{1}H NMR (600 MHz, DMSO-d_6) δ 8.89 (d, J = 6.8 Hz, 1H), 8.48 (dd, J = 4.8, 1.8 Hz, 1H), 8.24 (d, J = 2.5 Hz, 1H), 8.07 (s, 1H), 7.83 (s, 1H), 7.65 (dd, J = 7.5, 1.8 Hz,

1H), 7.38 (dd, J = 7.5, 4.8 Hz, 1H), 7.29 (d, J = 5.8 Hz, 4H), 7.25–7.17 (m, 1H), 6.21 (d, J = 2.6 Hz, 1H), 5.42 (m, 1H), 3.16 (dd, 13.9, 4.6 Hz, 1H), 2.86 (dd, J = 14.2, 8.9 Hz, 1H), 1.86–1.68 (m, 1H), 0.88–0.71 (m, 2H), 0.67–0.45 (m, 2H). ESI MS (m/z): calcd for $C_{22}H_{21}N_5O_3$, 403.2; found 404.2 [M + H^+].

***N*-(4-Amino-3,4-dioxo-1-phenylbutan-2-yl)-2-(3-(tetrahydro-2H-pyran-4-yl)-1*H*-pyrazol-1-yl)nicotinamide** (**33**). ^{1}H NMR (400 MHz, DMSO-d_6) δ 8.80 (d, J = 7.0 Hz, 1H), 8.49 (dd, J = 4.8, 1.8 Hz, 1H), 8.29 (d, J = 2.6 Hz, 1H), 8.00 (s, 1H), 7.80 (s, 1H), 7.67 (dd, J = 7.5, 1.8 Hz, 1H), 7.40 (dd, J = 7.6, 4.8 Hz, 1H), 7.33–7.18 (m, 5H), 6.36 (d, J = 2.6 Hz, 1H), 5.44 (m, 1H), 3.82 (dd, J = 11.5, 3.8 Hz, 2H), 3.78–2.5 (m, overlapping with water), 3.14 (dd, J = 14.0, 4.6 Hz, 1H), 2.83 (dd, J = 14.1, 8.8 Hz, 1H), 2.68 (m, 1H), 1.68 (m, 2H), 1.53 (m, 2H). ESI MS (m/z): calcd for $C_{24}H_{25}N_5O_4$, 447.2; found 448.2 [M + H^+].

***N*-(4-Amino-3,4-dioxo-1-phenylbutan-2-yl)-2-(3-(1-methylpiperidin-4-yl)-1*H*-pyrazol-1-yl)nicotinamide** (**34**). (9.6%) ^{1}H NMR (400 MHz, DMSO-d_6) δ 8.85 (d, J = 7.0 Hz, 1H), 8.51 (d, J = 4.9 Hz, 1H), 8.32 (d, J = 2.5 Hz, 1H), 8.11 (s, 1H), 7.86 (s, 1H), 7.68 (d, J = 7.6 Hz, 1H), 7.43 (dd, J = 7.6, 4.9 Hz, 1H), 7.38–7.09 (m, 5H), 6.38 (d, J = 2.5 Hz, 1H), 5.40 (m, 1H), 3.45-3.30 (dd, overlapping with water), 3.13. (dd, J = 14.0, 4.4 Hz, 1H), 2.82-2.48 (m, overlap with DMSO), 2.60 (s, overlapping with DMSO), 2.03-1.65 (m, 4H). ESI MS (m/z): calcd for $C_{25}H_{28}N_6O_3$, 447.2; found 460.2 [M + H^+].

***N*-(4-Amino-3,4-dioxo-1-phenylbutan-2-yl)-2-(3-benzyl-1*H*-pyrazol-1-yl)nicotinamide** (**35**). (65.2%) ^{1}H NMR (400 MHz, DMSO-d_6) δ 8.97 (d, J = 7.0 Hz, 1H), 8.50 (dd, J = 4.9, 1.7 Hz, 1H), 8.26 (d, J = 2.4 Hz, 1H), 8.03 (s, 1H), 7.80 (s, 1H), 7.70 (dd, J = 7.6, 1.7 Hz, 1H), 7.42 (dd, J = 7.5, 4.9 Hz, 1H), 7.31–7.13 (m, 10H), 6.24 (d, J = 2.5 Hz, 1H), 5.43 (m, 1H), 3.78 (s,

2H), 3.17 (dd, J = 14.2, 4.6 Hz, 1H), 2.90 (dd, J = 14.1, 8.8 Hz, 1H). ESI MS (m/z): calcd for $C_{26}H_{23}N_5O_3$, 453.2; found 454.2 [M + H^+].

***N*-(4-Amino-3,4-dioxo-1-phenylbutan-2-yl)-2-(4,5,6,7-tetrahydro-2H-indazol-2-yl)nicotinamide (36).** (63.5%) ^{1}H NMR (500 MHz, DMSO-d_6) δ 8.86 (d, J = 7.1 Hz, 1H), 8.46 (d, J = 4.9 Hz, 1H), 8.07 (s, 1H), 8.01 (s, 1H), 7.78 (s, 1H), 7.64 (d, J = 7.5 Hz, 1H), 7.35 (m, 1H), 7.30 -7.15 (m, 5H), 5.33 (m, 1H), 3.29–3.06 (dd overlapping with water, 1H), 2.91 (dd, J = 14.2, 8.8 Hz, 1H), 2.59–2.42 (m overlapping with DMSO, 4H), 1.69 (d, J = 18.7 Hz, 4H). ESI MS (m/z): calcd for $C_{23}H_{23}N_5O_3$, 417.2; found 418.2 [M + H^+].

***N*-(4-Amino-3,4-dioxo-1-phenylbutan-2-yl)-2-(3-(4-chlorophenyl)-1*H*-pyrazol-1-yl)nicotinamide (37)**. (55.3%) ^{1}H NMR (400 MHz, DMSO-d_6) δ 8.92 (d, J = 7.1 Hz, 1H), 8.55 (dd, J = 4.7, 1.8 Hz, 1H), 8.47 (d, J = 2.6 Hz, 1H), 8.08 (s, 1H), 7.86 (s, 1H), 7.76 (d, J = 8.3 Hz, 2H), 7.69 (m, 1H), 7.48 (m, 1H), 7.43 (d, J = 8.5 Hz, 2H), 7.23–7.08 (m, 5H), 7.02 (d, J = 2.6 Hz, 1H), 5.54 (m, 1H), 3.12 (dd, J = 14.1, 4.5 Hz, 1H), 2.76 (dd, J = 14.1, 9.1 Hz, 1H). ESI MS (m/z): calcd for $C_{25}H_{20}ClN_5O_3$, 473.1; found 474.1 [M + H^+].

***N*-(4-Amino-3,4-dioxo-1-phenylbutan-2-yl)-2-(3-(4-fluorophenyl)-1*H*-pyrazol-1-yl)nicotinamide (38**). (79%). ^{1}H NMR (500 MHz, DMSO-d_6) δ 8.94 (d, J = 7.1 Hz, 1H), 8.55 (dd, J = 4.7, 1.8 Hz, 1H), 8.46 (d, J = 2.7 Hz, 1H), 8.10 (s, 1H), 7.87 (s, 1H), 7.81 – 7.73 (m, 2H), 7.70 (dd, J = 7.6, 1.8 Hz, 1H), 7.46 (dd, J = 7.6, 4.8 Hz, 1H), 7.25–7.08 (m, 7H), 6.99 (d, J = 2.7 Hz, 1H), 5.76–5.32 (m, 1H), 3.13 (dd, J = 14.1, 4.4 Hz, 1H), 2.76 (dd, J = 14.1, 9.2 Hz, 1H). ^{13}C NMR (126 MHz, DMSO-d_6) δ 196.97, 166.95, 162.75, 151.93, 149.24, 147.41, 139.37, 137.63, 130.57, 129.45, 129.35, 128.62, 127.93, 127.86, 126.91, 124.49, 122.26, 116.03, 115.86, 105.64, 55.33, 36.04. ESI MS (m/z): calcd for $C_{25}H_{20}FN_5O_3$, 457.2; found 458.2 [M + H^+].

***N*-(4-Amino-3,4-dioxo-1-phenylbutan-2-yl)-2-(3-(4-methoxyphenyl)-1*H*-pyrazol-1-yl)nicotinamide (39).** (73.1%) ^{1}H NMR (400 MHz, DMSO-d_6) δ 8.91 (d, J = 7.1 Hz, 1H), 8.53 (dd, J = 4.9, 1.8 Hz, 1H), 8.43 (d, J = 2.7 Hz, 1H), 8.07 (s, 1H), 7.84 (s, 1H), 7.68 (dd, J = 7.9, 5.9 Hz, 3H), 7.43 (dd, J = 7.6, 4.8 Hz, 1H), 7.29–7.08 (m, 5H), 7.02–6.79 (m, 3H), 5.56 (m, 1H), 3.80 (s, 3H), 3.14 (dd, J = 14.1, 4.7 Hz, 1H), 2.79 (dd, J = 14.1, 8.9 Hz, 1H). ESI MS (m/z): calcd for $C_{26}H_{23}FN_5O_4$, 469.2; found 470.5 [M + H$^+$].

***N*-(4-Amino-3,4-dioxo-1-phenylbutan-2-yl)-2-(3-(4-(trifluoromethyl)phenyl)-1*H*-pyrazol-1-yl)nicotinamide (40)**. (50.2%). ^{1}H NMR (600 MHz, DMSO-d_6) δ 9.01 (d, J = 7.0 Hz, 1H), 8.58 (dd, J = 4.8, 1.8 Hz, 1H), 8.52 (d, J = 2.6 Hz, 1H), 8.17 (s, 1H), 7.94 (d, J = 8.1 Hz, 2H), 7.91 (s, 1H), 7.76–7.70 (m, 3H), 7.51 (dd, J = 7.6, 4.8 Hz, 1H), 7.21–7.07 (m, 6H), 5.54 (m, 1H), 3.15–3.09 (m, 1H), 3.12 (dd, J = 14.2, 4.3 Hz, 1H), 2.74 (dd, J = 14.1, 9.2 Hz, 1H). ESI MS (m/z): calcd for $C_{26}H_{20}F_3N_5O_3$, 507.2; found 508.2 [M + H$^+$].

***N*-(4-Amino-3,4-dioxo-1-phenylbutan-2-yl)-2-(3-(3-(trifluoromethyl)phenyl)-1*H*-pyrazol-1-yl)nicotinamide (41)**. (85.2%).1H NMR (400 MHz, DMSO-d_6) δ 8.89 (d, J = 6.8 Hz, 1H), 8.57 (dd, J = 4.9, 1.7 Hz, 1H), 8.49 (d, J = 2.6 Hz, 1H), 8.08 (s, 1H), 8.02 (d, J = 7.8 Hz, 1H), 7.96 (s, 1H), 7.84–7.72 (m, 2H), 7.68 (d, J = 7.9 Hz, 1H), 7.65–7.56 (m, 1H), 7.50 (dd, J = 7.7, 4.8 Hz, 1H), 7.15 (d, J = 2.6 Hz, 1H), 7.13–7.00 (m, 5H), 6.04–4.85 (m, 1H), 3.10 (dd, J = 14.2, 4.6 Hz, 1H), 2.75 (dd, J = 14.1, 9.0 Hz, 1H). ^{13}C NMR (126 MHz, DMSO-d_6) δ 196.84, 166.89, 162.88, 151.44, 149.35, 147.37, 139.50, 137.54, 133.90, 130.94, 130.17, 129.92, 129.59, 129.19, 128.46, 126.74, 125.71, 125.05, 124.70, 122.61, 122.31, 106.12, 55.80, 35.85. ESI MS (m/z): calcd for $C_{26}H_{20}F_3N_5O_3$, 507.2; found 508.2 [M + H$^+$].

***N*-(4-Amino-3,4-dioxo-1-phenylbutan-2-yl)-2-(3-(4-((diethylamino)methyl)phenyl)-1H-pyrazol-1-yl)nicotinamide (42)** (isolated as methanesulfonate - 52.3%). ^{1}H NMR (400 MHz,

DMSO-d_6) δ 9.26 (s, 1H), 8.90 (d, J = 6.7 Hz, 1H), 8.56 (dd, J = 4.8, 1.8 Hz, 1H), 8.49 (d, J = 2.7 Hz, 1H), 8.02 (s, 1H), 7.85 (d, J = 7.9 Hz, 3H), 7.80–7.72 (m, 2H), 7.54 (d, J = 7.9 Hz, 3H), 7.50 (m, 1H), 7.24–7.09 (m, 5H), 7.05 (d, J = 2.6 Hz, 1H), 5.50 (m, 1H), 4.34 (d, J = 5.3 Hz, 2H), 3.10 (m, 5H), 2.78 (dd, J = 14.2, 9.0 Hz, 1H), 2.30 (s, 3H), 1.34–1.16 (m, 6H). ESI MS (m/z): calcd for $C_{30}H_{32}N_6O_3$, 524.3; found 525.2 [M + H^+].

***N*-(4-Amino-3,4-dioxo-1-phenylbutan-2-yl)-2-(3-(4-(morpholinomethyl)phenyl)-1*H*-pyrazol-1-yl)nicotinamide (43)**. (27.2%) ^{1}H NMR (400 MHz, DMSO-d_6) δ 8.92 (d, J = 6.9 Hz, 1H), 8.54 (dd, J = 4.8, 1.7 Hz, 1H), 8.46 (d, J = 2.6 Hz, 1H), 8.03 (s, 1H), 7.81 (s, 1H), 7.76–7.62 (m, 3H), 7.46 (dd, J = 7.6, 4.8 Hz, 1H), 7.31 (d, J = 8.0 Hz, 2H), 7.23–7.08 (m, 5H), 6.97 (d, J = 2.6 Hz, 1H), 5.53 (m, 1H), 3.59 (t, J = 4.6 Hz, 4H), 3.48 (s, 2H), 3.12 (dd, J = 14.3, 4.7 Hz, 1H), 2.79 (dd, J = 14.2, 8.8 Hz, 1H), 2.36 (t, J = 4.5 Hz, 4H).). ESI MS (m/z): calcd for $C_{30}H_{30}N_6O_4$, 538.2; found 539.4 [M + H^+].

***N*-(4-Amino-3,4-dioxo-1-phenylbutan-2-yl)-2-(2H-indazol-2-yl)nicotinamide (44)**. (61.7%) ^{1}H NMR (400 MHz, DMSO-d_6) δ 9.09 (d, J = 7.1 Hz, 1H), 8.97 (s, 1H), 8.66 (dd, J = 4.8, 1.7 Hz, 1H), 8.07 (s, 1H), 7.85–7.81 (m, 2H), 7.79 (d, J = 8.5 Hz, 1H), 7.61 (dd, J = 7.6, 4.8 Hz, 1H), 7.51 (d, J = 8.8 Hz, 1H), 7.33–7.13 (m, 6H), 7.10 (dd, J = 8.6, 6.5 Hz, 1H), 5.38 (m, 1H), 3.15 (dd, J = 14.3, 4.4 Hz, 1H), 2.89 (dd, J = 14.3, 8.9 Hz, 1H). ESI MS (m/z): calcd for $C_{23}H_{19}N_5O_3$, 413.1; found 414.2 [M + H^+].

***N*-(4-Amino-3,4-dioxo-1-phenylbutan-2-yl)-2-(chromeno[4,3-c]pyrazol-2(4H)-yl)nicotinamide (45)**. (64.2%) ^{1}H NMR (400 MHz, DMSO-d_6) δ 9.02 (d, J = 6.9 Hz, 1H), 8.58–8.51 (m, 1H), 8.28 (s, 1H), 8.10 (s, 1H), 7.87 (s, 1H), 7.77–7.70 (m, 1H), 7.47 (dd, J = 7.5, 4.9 Hz, 1H), 7.37 (d, J = 7.5 Hz, 1H), 7.26 (t, J = 3.7 Hz, 1H), 7.27–7.14 (m, 5H), 6.98 (m, 2H), 5.48

(m, 1H), 5.31 (s, 2H), 3.15 (dd, J = 14.1, 4.7 Hz, 1H), 2.80 (dd, J = 14.1, 8.9 Hz, 1H). ESI MS (m/z): calcd for $C_{26}H_{21}N_5O_4$, 467.2; found 468.2 [M + H^+].

Biochemical assays: Inhibition of human calpain 1 activity was determined in a kinetic fluorescence assay using 20 nM erythrocyte calpain 1 (Calbiochem #208713) and 100 μM Suc-Leu-Tyr-AMC (Bachem #I-1355) as a substrate in 62 mM imidazole, 0.3 mM CaCl2, 0.10% CHAPS, 0.05% BSA, 1 mM DTT, pH 7.3 at room temperature. Inhibition of cathepsins B, K, L and S was determined in a kinetic fluorescence assay: human cathepsin B activity using 0.25 nM cathepsin B from human liver (Calbiochem #219362) and 100 μM Z-Phe-Arg-AMC (Bachem #I-1160) as a substrate in 50 mM MES, 2 mM EDTA, 0.05% Brij 35, 2.5 mM L-cysteine, pH 6.0 at room temperature; human cathepsin K activity using 3 nM cathepsin K activated from recombinant human procathepsin K expressed in E.coli (Calbiochem #342001) and 10 μM Z-Gly-Pro-Arg-AMC (Biomol #P-142) as a substrate in 50 mM MES, 2 mM EDTA, 0.05% Brij 35, 2.5 mM L-cysteine, pH 6.0 at room temperature; human cathepsin L activity using 1 nM cathepsin L from human liver (Calbiochem #219402) and 2 μM Z-Phe-Arg-AMC (Bachem #I-1160) as a substrate in 50 mM MES, 2 mM EDTA, 0.05% Brij 35, 2.5 mM L-cysteine, pH 6.0 at room temperature; human cathepsin S activity using 0.5 nM recombinant human cathepsin S expressed in E.coli (Calbiochem #219343) and 20 μM Z-Val-Val-Arg-AMC (Bachem #I-1540) as a substrate in 50 mM MES, 2 mM EDTA, 0.05% Brij 35, 2.5 mM L-cysteine, pH 6.0 at room temperature.

Assuming simple competitive inhibition, the Cheng-Prusoff equation was used to calculate Ki values from the IC_{50} values. The Km values determined under the assay conditions listed above were 210 μM (Suc-Leu-Tyr-AMC and calpain-1), 90 μM (Z-Phe-Arg-AMC and cathepsin B), 10 μM (Z-Gly-Pro-Arg-AMC and cathepsin K), 2 μM (Z-Phe-Arg-AMC and cathepsin L), and 30

μM (Z-Val-Val-Arg-AMC and cathepsin S). The Ki values are means of the inhibition constants calculated from data of two to four independent concentration response curves.

Assessment of *in-vitro* racemisation. *Preparation of hirudin-anticoagulated rat plasma:* Blood samples (0.9 ml) were drawn from the catheterized carotid artery of anaesthetized rats into 0.1 mL of 1 μM recombinant hirudin (Fluka # 94581) dissolved in isotonic saline. Samples were mixed gently and centrifuged for 5 min at 5000 x g at 4°C. The supernatant plasma was collected and immediately used for the experiments as described below.

Assessment of enantiomer racemization in buffer or rat plasma in vitro: Determinations of apparent Ki values for human calpain-1 were performed in imidazol assay buffer or hirudin-anticoagulated rat plasma spiked with either compound **(*S*)-19** (active enantiomer) or ***(R)*-19** (inactive enantiomer) to a final concentration of 1 mM. After the desired period of incubation (0–360 min at 37°C), aliquots were taken and diluted serially to yield final concentrations from 1 μM down to 0.03 nM calculated on the basis of the initial test compound concentration. The apparent Ki for calpain 1 inhibition was determined as described.

Evaluation of racemization velocity: Compound **19** and its enantiomers were tested at ten concentrations in half-log increments in the calpain 1 assay, and inhibition of product formation was determined. The concentration of each compound required to inhibit activity by 50% (IC_{50}) was determined from the inhibition curve by non-linear regression analysis (GraphPad Prism®) of all data points including the control activity in presence of solvent instead of compound solution and background signal in the absence of enzyme. Assuming competitive inhibition when Hill slopes were close to 1, Ki values were calculated from these IC_{50} values and the previously determined Km for Suc-Leu-Tyr-AMC using the Cheng-Prusoff equation. Means and 95% confidence limits of Ki determinations were obtained using standard statistical methods. Half

lifes of racemization were determined by nonlinear fitting of apparent Ki values to a one-phase exponential decay with Y=Span*exp(-K*X)+Plateau, which starts at Span+Plateau and decays to Plateau with a shared rate constant K. The half lifes are 0.96/K.

Reversibility of calpain inhibition. Human calpain 1 was incubated for 30 min with the inhibitor or solvent to allow complete equilibration. Excess inhibitor was removed by a P-30 column passage and the flow-through diluted into a calpain activity assay and cleavage of fluorogenic substrate was monitored continuously for 2 hours. The time course data were fitted to: P=offset+Vs*t+(Vi-Vs)/Koff*(1-exp(-Koff*t)) with Vs=7.6 determined in parallel control experiments.[61]

Assessment of cellular calpain activity *in-vitro*. *NMDA-induced spectrin degradation in hippocampal slice cultures*: Organotypic slice cultures were cultivated in medium containing 2% serum for 6-8 days before experimentation. In initial experiments the effect on spectrin cleavage by different NMDA concentrations was studied. The incubation of hippocampal slices for 5 hours (34°C, 5% CO_2) with 10 μM of NMDA resulted in significant spectrin cleavage. Appearance of spectrin degradation products in the 150/145 kDa range were detected by density quantified Western blotting after lysis of the slices in tissue homogenation buffer (50 mM Tris-HCl (pH 7.4), 150 mM NaCl, 5 mM EDTA, 10% Sucrose, 0.10% CHAPS, 2 mM DTT, 1:25 cOmplete™ protease inhibitor cocktail (Roche), and 1:100 phosphatase inhibitor cocktail (Calbiochem)) using an anti-spectrin alpha chain antibody (clone AA6, MAB1622, Chemicon). To determine the prevention of spectrin degradation, slice cultures were pre-incubated for 30 min with inhibitor followed by addition of NMDA.

NMDA-induced tau degradation: Following the experimental procedure as described above, formation of the 17kD tau cleavage product was detected by density quantified Western blotting

after lysis of the slices in tissue homogenation buffer (50 mM Tris-HCl (pH 7.4), 150 mM NaCl, 5 mM EDTA, 10% Sucrose, 0.10% CHAPS, 2 mM DTT, 1:25 cOmplete™ protease inhibitor cocktail (Roche), and 1:100 phosphatase inhibitor cocktail (Calbiochem)) using an anti-Tau 1 antibody (clone PC1C6, MAB3420, Chemicon).

Electrophysiological recordings in slice cultures: Hippocampal slice cultures were prepared from 9- to 10-day-old Wistar rats (Janvier, Genest St.Ile, France). Hippocampi were isolated, and transverse hippocampal slices (400 μM thickness) were prepared as described in the literature.[62] Slices were cultured for 15–18 days before recording. For oligomer experiments, 82 nM $A\beta_{1-42}$ globulomer (prepared according to the literature)[55] was applied to medium 1 day before recording. In the compound group, compound **38** was co-applied. One group was only treated with vehicle. At least 1 hour before recording slice cultures were placed in a Haas interface recording chamber (Harvard Apparatus, USA) and continuously perfused with artificial cerebrospinal fluid (aCSF; in mM: NaCl, 118; KCl, 5; $MgSO_4$, 2; $CaCl_2$, 2.5; KH_2PO_4, 1.24; $NaHCO_3$, 25.6; glucose, 10; pH 7.5. The Schaffer collateral was then stimulated, and extracellular field potential (fEPSP) amplitudes were recorded and signals digitized using a power CED 1401 (Cambridge Electronic Design Ltd, Cambridge, UK). For statistical analysis a 2-way repeated measures analysis of variance (ANOVA) with all pairwise multiple comparison procedures (Holm-Sidak method) was applied.

Formulation of compound 38: For oral administration the compound was dissolved in Cremophor EL and Capmul PG8 (20:80 v/v), for subcutaneous administration a mixture of ethanol, PEG400 and sterile water (20:30:50 v/v/v) was used as vehicle.

Microdialysis: Male Sprague Dawley rats (Janvier, France) were maintained under standard conditions (12 hours day/night cycle, light switched on at 06:00 a.m., room temperature 22°C,

50% humidity) with free access to food and tap water. Before being used for the experiments, animals were allowed to recover from transportation for at least one week. All experiments were conducted during the light period of the light/dark cycle.

Surgery and microdialysis: For pain prophylaxis Carboprofen (3 mg/kg, i.p; Rimadyl®, Pfizer, Germany) was administered before surgery. Individual male Sprague-Dawley rats (290 – 320 g body weight) anesthetized with pentobarbital (60 mg/kg, i.p, Narcoren®, Rhone-Merieux GmbH, France) were mounted in a KOPF stereotaxic frame for the implantation of two microdialysis guide cannula (CMA/12, Axel Semrau GmbH, Germany). One guide cannula was implanted into the medial prefrontal cortex (AP = 2.5; ML = 0.6; DV = -0.2) and the second into the hippocampus (AP = 5.5; ML = 4.5; DV = -4.5). The guide cannula were secured with dental cement (Technovit powder, Product No 5071, Technovit polymerization starter fluid, Product No 2060, Kulzer GmbH, Dormagen, Germany) and four anchor screws into the skull. Rats were allowed to recover from surgery for five to seven days. The day before the experiment, each animal was transferred into a system allowing for free movement [CMA/120 Axel Semrau GmbH, Germany, consisting of a plastic bowl (diameter 400 mm at the top), wire attachment, counter-balance arm, swivel assembly connecting in-/outlet of the probe with the perfusion pump]. Next, a CMA/12 microdialysis probe (3 mm membrane length, Axel Semrau GmbH, Germany) was slowly lowered into the final position. The probe was perfused with Ringer solution (147 mM NaCl, 4.0 mM KCl and 2.4 mM $CaCl_2$, containing 1 µM neostigmine), for about 1 hour (CMA/102 microdialysis pump, Axel Semrau GmbH, Germany; 1.5 µL/min). The probe was perfused again 24 hours later for at least 1 hour before microdialysate fractions were collected every 20 minutes. Six fractions before and six fractions after administration of

compound **38** (1; 3; 10 mg/kg, s.c.) or vehicle were analyzed for microdialysate levels of acetylcholine by HPLC with electrochemical detection.

Assay of Microdialysate Acetylcholine Levels: 10 µL of each microdialysate fraction was injected onto a reversed phase column (MF 8908 Acetylcholine SepStik Kit; microbore column, particle size 10 µm, 530 x 1.0 mm coupled to an immobilized enzyme reactor 50 x 1.0 mm, particle size 10 µm, containing acetylcholine esterase and choline oxidase; BAS, U.S.A.) using a refrigerated autosampler (HTC PAL twin injector autosampler system, Axel Semrau, Germany). The mobile phase consisted of 50 mmol/L Na_2HPO_4 (pH 8.5) and 5 mL/L ProClin® (1 %, v/v, microbiocide, BAS, U.S.A.). Flow rate was 0.14 mL/min (Rheos Flux pump, Axel Semrau GmbH, Germany), and the sample run time was less than 15 minutes. Acetylcholine and choline were measured via an electrochemical detector (LC-4C, BAS, Lafayette, IN) with a platinum working electrode set at + 500 mV versus an Ag/AgCl reference electrode. The system was calibrated by standard solutions (acetylcholine, choline) containing 1 pmol/10 µL injection. Acetylcholine was identified by its retention time and peak height with an external standard method using chromatography software (Chrom Perfect®, version 4.4.22, Justice Laboratory Software, U.S.A.). Microdialysis (area under curve data collapsed over 0 - 120 min based on percent baseline change) data were evaluated for significance using one-way analysis of variance (ANOVA) followed by Dunnett's multiple comparison post hoc test using GraphPad Prism v 5.0 software. Statistical significance was defined as $p < 0.05$.

E-Phys/Sleep EEG: Male Fisher rats (250-330g, Charles River, Sulzfeld, Germany) were implanted with EEG electrodes (frontal = Bregma +1.5mm, lateral +1,5mm and Occipital Lambda -1.5mm, lateral 1.5mm). Therefore, animals were anaesthetized with Ketavet® (Ketamine, 25mg/kg) and Narcoren® (Pentobarbital 30mg/kg); for pain treatment animals

received Rimadyl ® (Carboprofen, 4mg/kg) for 3 days after surgery. After transfer into a stereotactic frame (David Kopf, model 961, Tujunga, California) the skin above the skull was opened by incision. Small holes were drilled into the skull. Damage of the meninges was carefully avoided. Custom made teflon-coated steel electrodes were placed in the burr holes and glued to the skull with dental cement (Technovit 2060, Heraeus Kulzer, Germany). The skin was closed around the implanted electrode connector. Animals were allowed to recover from surgery for at least 2 weeks before going into first experiments. For habituation animals were transferred into the EEG recording chamber repeatedly before the first experiments started. All animals were acclimated to the animal facilities for a period of at least one week prior to surgery. Food and water were available ad libitum. Animals were tested in the light phase of a 12-hour light: 12-hour dark schedule (lights on at 05:30 hours). Immediately before recording animals received compound **38** by gavage and were then transferred into the recording chamber and connected to the EEG system. Four animals (2 substance-treated and 2 controls) were recorded at the same day for 8 hours starting at the beginning of the light period. In the experimental cross-over design the same animals received alternative treatment one week later. During recording the animals were deprived of food and water. REM parameters and total sleep time were analyzed. Data were analyzed by GraphPad Prism V5.0 (GraphPad Software, Inc., San Diego, CA USA). Each dose investigated was analyzed as an individual sub-experiment. Due to the crossover design each animal was used as its own control. Therefore, a paired t-test was used for analysis of the data. Statistical significance was defined as $p<0.05$.

Scopolamine-induced Deficits in Passive Avoidance Responding: Male Wistar rats were obtained from Harlan Laboratories, The Netherlands, and group-housed 2 per cage (42.5 x 26.6 x 15.5 cm). The age upon arrival was 11 weeks. All animals were acclimated to the animal

facilities for a period of at least one week prior to the commencement of experimental procedures. Food and water were available ad libitum. Animals were tested in the light phase of a 12-hour light: 12-hour dark schedule (lights on at 0600 hours for social recognition experiments and 0530 hours for the passive avoidance experiments). In the experimental apparatus (Rat Shuttle Cage, Coulburn Instruments, Whitehall, PA) rats received one single training session. The animals were placed into the brightly lit compartment of the shuttle box (53x28.5x26 cm as measured from the raised grid floor) with the guillotine door closed. After a habituation period of 2 min, the guillotine door opened, allowing the animals to cross to the dark compartment of the cage. Once the animals moved into the dark compartment, the guillotine door closed and a single footshock (0.5 mA, 2 sec) was delivered. The trial was then terminated and the animal returned to its home cage. After a 24-hour retention period, the animals were placed back into the bright compartment of the shuttle box and the latency to enter the dark, previously shocked compartment was measured. GraphPad Prism (version 5.0, GraphPad Software, San Diego CA, USA) was used to analyze the data. Data were analyzed using an analysis of variance (ANOVA) with drug treatment as a between subject factor followed by Dunnett's post-hoc comparison. Whenever appropriate, an unpaired Student t-test was used to analyze the effects of physostigmine in scopolamine-induced deficits in passive avoidance responding. Alpha was set at 0.05.

Animal welfare: All experiments in laboratory animals were approved by the government of Rhineland Platinate (Landesuntersuchungsamt Koblenz) and conducted in accordance with the German Animal Welfare Act and the Guide for the Care and Use of Laboratory Animals (2011). The facilities are accredited by the Association for Assessment and Accreditation of Laboratory Animal Care (AAALAC International).

ASSOCIATED CONTENT

Supporting Information. The Supporting Information is available free of charge on the ACS Publications website:

Molecular formula strings (CSV)

Homology model (PDB file)

Recovery of calpain 1 activity after pre-incubation with compound **19**; homology model of compound **19** in human calpain 1 and cathepsin K with close-up on the S3 site; racemization of (R)- and (S)-**19** under physiological conditions at 37°C; profiles of compound **19** in a CEREP panel of 74 receptor binding assays and the MDS EnzymeProfilingScreen of 82 enzymes; profiles of compound **38** in a CEREP panel of 74 receptor binding assays and the MDS EnzymeProfilingScreen of 81 enzymes; ^{1}H NMR and ^{13}C spectra for compounds **19** and **38** (PDF).

AUTHOR INFORMATION

Corresponding Author

* Phone: +49(0)621-5893449; E-mail: andreas.kling@abbvie.com

Present Addresses

⊥ For Y. L.: Eli Lilly and Company; Lilly Corporate Center, Indianapolis IN 46285 U.S.A. For V. N.: AbbVie Deutschland GmbH & Co. KG, DMPK-TM Development Sciences, Knollstrasse, 67061 Ludwigshafen, Germany.

Notes

[#] K. D., A. M. and Y. L. are former AbbVie employees.

The authors declare the following competing financial interest(s): The authors are current or former employees of AbbVie (or Abbott Laboratories prior to separation), and may own company stock.

ACKNOWLEDGMENT

We thank the global Abbott/AbbVie calpain project team, in particular A. Boehler, J. Froggett, S. Heitz, S. Maurus, V. Ott and C. Thiem for synthesis, C. Krack and the LU team and C. J. Chen from NC for analytical support.

Design, study conduct, and financial support for this research was provided by AbbVie. AbbVie participated in the interpretation of data, review, and approval of the publication.

ABBREVIATIONS

AMC, 7-amino-4-methylcoumarin; BZD, benzodiazepine; Cal, calpain; Cat, cathepsin; CHAPS, 3-[(3-cholamidopropyl)dimethylammonio]-1-propanesulfonate; EDCI, 1-ethyl-3-(3-dimethylaminopropyl)carbodiimide; EtOAc, ethylacetate; EtOH, ethanol; fsp3, fraction sp3 carbon; GCPR, G protein-coupled receptor; hERG, human Ether-a-go-go Related Gene; HOBt, hydroxybenzotriazole; HSC, hippocampal slice cultures; MeOH, methanol; MES, 2-(N-

morpholino)ethanesulfonic acid; NMDA, N-methyl-D-aspartate; PEPPSI-IPr [1,3-Bis(2,6-Diisopropylphenyl)imidazol-2-ylidene](3-chloropyridyl)palladium(II) dichloride PyBr3, Pyridinium tribromide; SDP, spectrin degradation product; Suc, succinyl; TPSA, topological polar surface area.

REFERENCES

(1) Goll, D. E.; Thompson, V. F.; Hongoi, L.; Wei, W.; Congdarerel, J. The Calpain System. *Physiol. Rev*. **2003**, *83*, 731-801.

(2) Huang, Y.; Wang, K. K. W. The Calpain Family and Human Disease. *Trends Mol. Med*. **2001**, *7*, 355-362.

(3) Ono, Y.; Saido, T. C.; Sorimachi, H.; Calpain Research for Drug Discovery: Challenges and Potential. *Nat. Rev. Drug Discovery* **2016**, 854-876.

(4) Potz, B. A.; Abid, M. R.; Selke, F. W. Role of Calpain in Pathogenesis of Human Disease Processes. *J. Nat. Sci.* **2016**, *2*, e218.

(5) LaFerla, F. M.; Querfurth, H. W. Alzheimer´s Disease. *N. Engl. J. Med.* **2010**, *362*, 329-344.

(6) Tsuji, T.; Shimohamaa, S.; Kimuraa, J.; Shimizu, K. m-Calpain (Calcium-activated Neutral Proteinase) in Alzheimer's Disease Brains. *Neurosci. Lett.* **1998**, *248*, 109-112.

(7) Saito, K.; Elce, J. T.; Hamos, J. E.; Nixon, R. A. Widespread Activation of Calcium-activated Neutral Proteinase (Calpain) in the Brain in Alzheimer Disease: A Potential Molecular Basis for Neuronal Degeneration. *Proc. Natl. Acad. Sci. U.S.A*- **1993**, *90*, 2628-2632.

(8) Ferreira, A. Calpain Dysregulation in Alzheimer's Disease. *ISRN Biochem.* **2012**, *2012,* 728571.

(9) Kelly, B. L.; Ferreira, A. Beta-Amyloid Disrupted Synaptic Vesicle Endocytosis in Cultured Hippocampal Neurons. *Neuroscience* **2007**, *147*, 60-70.

(10) Higuchi, M.; Tomioka, M.; Takano, J.; Shirotani, K.; Iwata, N.; Masumoto, H.; Maki, M.; Saido, T. C. Distinct Mechanistic Roles of Calpain and Caspase Activation in Neurodegeneration as Revealed in Mice Overexpressing their specific inhibitors. *J. Biol. Chem*. **2005**, *280*, 15229-15237.

(11) Battaglia, F.; Trinchese, F.; Liu, S. Walter, S.; Nixon, R. A.; Arancio, O. Calpain Inhibitors: A Treatment for Alzheimer´s Disease. *J. Mol. Neurosci.* **2003**, *20*, 357-362.

(12) Chiu, K.; Lama, T. T.; Lia, W. W. J.; Capriolid, J.; Kwong, J. M. K. Calpain and N-methyl-d-aspartate (NMDA)-induced Excitotoxicity in Rat Retinas. *Brain Res.* **2005**, *1046*, 207-215.

(13) Wu, H. Y.; Tomizawa, K.; Oda, Y; Wei, F. Y.; Lu, Y. F.; Matsushita, M.; Li, S. T.; Moriwaki, A.; Matsui, H. Critical Role of Calpain-mediated Cleavage of Calcineurin in Excitotoxic Neurodegeneration. *J. Biol. Chem*. **2004**, *279*, 6, 4929-4940.

(14) Lee, M.; Kwon, Y. T.; Li, M.; Peng, J.; Friedlander, R.M.; Tsai, L. Neurotoxicity Induces Cleavage of p35 to p25 by Calpain. *Nature* **2000**, *140*, 360-364.

(15) Monaco, E. A. Recent Evidence Regarding a Role for Cdk5 Dysregulation in Alzheimer's Disease. *Curr. Alzheimer Res.* **2004**, *1*, 33-38.

(16) Trinchese, F.; Fa, M.; Liu, S.; Zhang, H.; Hidalgo, A.; Schmidt, S.D.; Yamaguchi, H.; Yoshii, N.; Mathews, P.M.; Nixon, R.A.; Arancio, O. Inhibition of Calpains Improves Memory and Synaptic Transmission in a Mouse Model of Alzheimer Disease. *J. Clin. Invest*. **2008**, *118*, 2796-2807.

(17) Rao, M. V.; McBrayer, M. K.; Campbell, J.; Kumar, A.; Hashim, A.; Sershen, H.; Stavrides, P. H.; Ohno, M.; Hutton, M.; Nixon, R. A. Specific Calpain Inhibition by Calpastatin Prevents Tauopathy and Neurodegeneration and Restores Normal Lifespan in Tau P301L Mice. *J. Neurosci*. **2014**, *34*, 9222–9234.

(18) Liang, B.; Duan, B.; Zhou, X.; Gong, J.; Luo, Z. Calpain Activation Promotes BACE1 Expression, Amyloid Precursor Protein Processing, and Amyloid Plaque Formation in a Transgenic Mouse Model of Alzheimer Disease. *J. Biol. Chem*. **2010**, *285*, 27737–27744.

(19) Ray, S. K.; Banik, N. L. Calpain and its Involvement in the Pathophysiology of CNS Injuries and Diseases. *Curr. Drug Targets: CNS Neurol. Disord.* **2003**, *2*, 173-189.

(20) Camins, A.; Verdaguer, E.; Folch, J.; Pallàs, M. Involvement of Calpain Activation in Neurodegenerative Processes. *CNS Drug Rev.* **2006**, *12*, 135–148

(21) Liu, J.; Liu, M. C.; Wang, K. W. K. Calpain in the CNS: From Synaptic Function to Neurotoxicity. *Sci. Signaling* **2008**, *1,* re1.

(22) Pietsch, M.; Krystle, C. H.; Abell, C.; Abell, A. D. Calpains: Attractive Targets for the Development of Synthetic Inhibitors. *Curr. Top. Med. Chem.* **2010**, *10*, 270-293.

(23) Donkor, I. Calpain Inhibitors: A Survey of Compounds Reported in the Patent and Scientific Literature. *Expert Opin. Ther. Pat*. **2011**, *21*, 601-636.

(24) Schiefer, I. T.; Subhasish, T.; Litosh, V.; Siklos, M.; Scism, R.; Wijewickrama, G. T.; Chandrasena, E. P.; Sinha, V.; Tavassoli, E.; Brunsteiner, M.; Fa, M.; Arancio, O.; Petukhov, P.; Thatcher, G. R. J. Design, Synthesis, and Optimization of Novel Epoxide Incorporating Peptidomimetics as Selective Calpain Inhibitors. *J. Med. Chem*. **2013**, *56*, 6054−6068.

(25) Donkor, I. An Updated Patent Review of Calpain Inhibitors (2012 -- 2014). *Expert Opin. Ther. Pat*. **2014**, *25*, 17-31.

(26) Lubisch, W.; Beckenbach, E.; Bopp, S.; Hofmann, H.P.; Kartal, A.; Kaestel, C.; Lindner, T.; Metz-Garrecht, M.; Reeb, J.; Regner, F.; Vierling, M.; Moeller, A. Benzoylalanine-Derived Ketoamides Carrying Vinylbenzyl Amino Residues: Discovery of Potent Water-Soluble Calpain Inhibitors with Oral Bioavailability. *J. Med. Chem*. **2003**, *46*, 2404-2412.

(27) Neuhof, C.; Fabiunke, V.; Deibele, K.; Speth, M.; Moeller, A.; Lubisch, W.; Fritz, H.; Tillmanns, H.; Neuhof, H. Reduction of Myocardial Infarction by Calpain Inhibitors A-705239 and A-705253 in Isolated Perfused Rabbit Hearts. *Biol. Chem*. **2008**, *385*, 1077–1082.

(28) Khalil, P. N.; Neuhof, C.; Huss, R.; Pollhammer, M.; Khalil, M. N.; Neuhof, H.; Fritz, H.; Siebeck, M. Calpain Inhibition Reduces Infarct Size and Improves Global Hemodynamics and Left Ventricular Contractility in a Porcine Myocardial Ischemia/Reperfusion Model. *Eur. J. Pharm*. **2005**, *528*, 124–131.

(29) Randriamboavonjy, V.; Isaak, J.; Elgheznawy, A.; Pistrosch, F.; Froemel, T.; Yin, X.; Badenhoop, K.; Heide, H.; Mayr, H.; Fleming, I. Calpain Inhibition Stabilizes the Platelet Proteome and Reactivity in Diabetes. *Blood* **2012**, *120*, 415-423.

(30) Drescher, K. U., Browman, K. E.; Wicke, K. W.; Kling, A., Gross, G.; Moeller, A. Effect of Calpain Inhibition on Acetylcholine Release and Social Recognition. *Poster at the 40th Annual Meeting of the Society for Neuroscience*, San Diego, November 13-17 2010.

(31) Sinjoanu, R. C.; Kleinschmidt, S.; Bitner, R. S.; Brioni, J. D.; Moeller, A.; Ferreira, A. The Novel Calpain Inhibitor A-705253 Potently Inhibits Oligomeric beta-Amyloid-induced Dynamin 1 and Tau Cleavage in Hippocampal Neurons. *Neurochem. Int.* **2008**, *53*, 79–88.

(32) Nimmrich, V.; Szabo, R.; Nyakas, C.; Granic, I.; Reymann, K. G.; Schroeder, U. H.; Gross, G.; Schoemaker, H.; Wicke, K.; Moeller, A.; Luiten, P. Inhibition of Calpain Prevents N-Methyl-D-aspartate-Induced Degeneration of the Nucleus Basalis and Associated Behavioral Dysfunction. *J. Pharmacol. Exp. Ther*. **2008**, *327*, 343–352.

(33) Granic, I.; Nyakas, C.; Luiten, P. G. M.; Eisel, U. L. M.; Halmy, L. G.; Gross, G.; Schoemaker, H.; Moeller, A.; Nimmrich, V. Calpain Inhibition Prevents Amyloid-β-induced Neurodegeneration and Associated Behavioral Dysfunction in Rats. *Neuropharmacology* **2010**, *59*, 334-342.

(34) Nikkel, A. L.; Martino, B.; Markosyan, S.; Brederson, J.; Medeiros, R.; Moeller, A.; Bitner, R. S. The Novel Calpain Inhibitor A-705253 Prevents Stress-induced Tau Hyperphosphorylation in vitro and in vivo. *Neuropharmacology* **2012**, *63*, 606-612.

(35) Medeiros, R.; Kitazawa, M.; Chabrier, M. A.; Cheng, D.; Baglietto-Vargas, D.; Kling, A.; Moeller, A.; Green, K. N.; LaFerla, F. M. Calpain Inhibitor A-705253 Mitigates Alzheimer's Disease–Like Pathology and Cognitive Decline in Aged 3xTgAD Mice. *Am. J. Pathol*. **2012**, *181*, 616-625.

(36) Reiser, J.; Adair, B; Reinheckel, T. Specialized Roles for Cysteine Cathepsins in Health and Disease. *J. Clin. Invest*. **2010**, *120,* 3421–3431.

(37) Turk, V.; Stoka, V.; Vasiljeva, O.; Renko, M.; Sun, T.; Turk, B.; Turk, D. Cysteine Cathepsins: From Structure, Function and Regulation to New Frontiers. *Biochim. Biophys. Acta* **2012**, *1824*, 68–88.

(38) Broemme, D.; Lecaille, F. Cathepsin K Inhibitors for Osteoporosis and Potential Off-target Effects. *Expert Opin. Invest. Drugs* **2009**, *18*, 585-600.

(39) Reinheckel, T.; Deusing, J.; Roth, W.; Peters, C. Towards Specific Functions of Lysosomal Cysteine Proteases: Phenotypes of Mice Deficient for Cathepsin B or Cathepsin L. *Biol. Chem*. **2001**, *382*, 735-741.

(40) Mueller-Steiner, S.; Zhou, Y.; Arai, H.; Roberson, E. D., Sun, B.; Chen, J.; Wang, X.; Yu, G.; Esposito, L.; Mucke, L.; Gan, L. Antiamyloidogenic and Neuroprotective Functions of Cathepsin B: Implications for Alzheimer's Disease. *Neuron* **2006**, *51*, 703–714.

(41) (a) Lubisch, W.; Moeller, A.; Treiber, H. J.; Knopp, M. Heterocyclically Substituted Amides Used as Calpain Inhibitors. *WO 9954305* 1999. (b) Lubisch, W.; Moeller, A.; Treiber, H. J.; Knopp, M. New Heterocyclically Substituted Amides, Their Production and Their Use. *WO 9961423* 1999.

(42) Tidwell, T. T. Oxidation of Alcohols to Carbonyl Compounds via Alkoxysulfonium Ylides: The Moffatt, Swern, and Related Oxidations. *Org. React*. **1990**, *39*, 297-572.

(43) Pleier; A. K.; Glas, H.; Grosche, M.; Sirsch, P.; Thiel, W. R. Microwave Assisted Synthesis of 1-Aryl-3-dimethylaminoprop-2-enones: A Simple and Rapid Access to 3(5)-Arylpyrazoles. *Synthesis* **2001**, *1*, 55–62.

(44) Wang, Z. Hantzsch Thiazole Synthesis. In *Comprehensive Organic Name Reactions and Reagents,* 1st ed.; Wang, Z., Ed.; John Wiley & Sons, Inc.: New York, 2010; pp 1330–1334.

(45) Suzuki, A. Cross-coupling Reactions via Organoboranes. *J. Organomet. Chem.* **2002**, *653*, 83–90.

(46) Harbeson, S. L.; Abelleira, S. M.; Akiyama, A.; Barrett, R. Carroll, R. M.; Straub, J. A.; Tkacz, J. N.; Wu, C.; Musso, G. F. Stereospecific Synthesis of Peptidyl α-Keto Amides as Inhibitors of Calpain. *J. Med. Chem*. **1994**, *37*, 2918-2929.

(47) Pellacini, F; Chiarino, D.; Carenzi, B. A. Diastereoselective Process for the Preparation of Intermediates for the Synthesis of Peptide Derivatives. US 5,157,143 1992.

(48) PDB 1TL9: Moldoveanu, T.; Campbell, R. L.:; Cuerrier, D.; Davies, P. L. Crystal Structures of Calpain–E64 and –Leupeptin Inhibitor Complexes Reveal Mobile Loops Gating the Active Site. *J. Mol. Biol.* **2004**, *343*, 1313–1326.

(49) PDB 1MEM: McGrath, M. E.; Klaus, J. L., Barnes, M. G.; Brömme, D. Crystal structure of human cathepsin K complexed with a potent inhibitor. *Nat. Struct. Biol*. **1997**, *4*, 105-109.

(50) Lovering, F.; Bikker, J.; Humblet, C. Escape from Flatland: Increasing Saturation as an Approach to Improving Clinical Success. *J. Med. Chem*. **2009**, *52*, 6752-6756.

(51) Observed Ki (***R*)-19** = 123nM; a fraction of 5% S-enantiomere was determined via chiral HPLC, hence a Ki value of >5000nM for (***R)*-19** can be extrapolated.

(52) Huth, J. R.; Mendoza, E.; Olejniczak, E. T.; Johnson, R. W.; Cothron, D. A.; Liu, Y.; Lerner, C. G.; Chen, J.; Hajduk, P. J.ALARM NMR: A Rapid and Robust Experimental Method To Detect Reactive False Positives in Biochemical Screens. *J. Am. Chem. Soc.* **2005**, *127*, 217-224.

(53) Hoffmann, F.; Maser, E. Carbonyl Reductases and Pluripotent Hydroxysteroid Dehydrogenases of the Short-Chain Dehydrogenases/Reductases Superfamily. *Drug Metab. Rev.* **2007**, 39, 87-144.

(54) Chesser, A. S.; Pritchard, S. M.; Johnson, G. V. W.; Tau Clearance Mechanisms and Their Possible Role in the Pathogenesis of Alzheimer´s Disease. *Front. Neurol*. **2013**, *4*, 1-12.

(55) Barghorn, S.; Nimmrich, V.; Striebinger, A.; Krantz, C.; Keller, P.; Janson, B.; Bahr, M.; Schmidt, M.; Bitner, R. S.; Harlan, J.; Barlow, E.; Ebert, U.; Hillen, H. Globular Amyloid beta-Peptide Oligomer - A Homogenous and Stable Neuropathological Protein in Alzheimer's Disease. *J. Neurochem.* **2005**, *95*, 834-847.

(56) Morales, W.; Poyares, D. R.; Guilleminault, C.; Ramos, L. R.; Bertolucci, P. H. F.; Tufik, S. The Effect of Donepezil on Sleep and REM sleep EEG in Patients with Alzheimer Disease: A Double-Blind Placebo-Controlled Study. *Sleep* **2006**, *29*, 199-205.

(57) Kling, A.; Jantos, K.; Mack, H.; Backfisch, G.; Lao, Y.; Nijssen, M.; Hornberger, W. Moeller, A. *Unpublished results.*.

(58) Kling, A.; Hornberger, W.; Mack, H.; Moeller, A.; Nimmrich, V.; Seemann, D.; Lubisch, W. Carboxamide compounds and Their Use as Calpain Inhibitors. *WO 2008080969*, 2008.

(59) Kling, A.; Jantos, K.; Mack, H.; Hornberger, W.;.Moeller, A.; Backfisch, G.; Lao, Y.; Nijsen, M. Carboxamide Compounds and Their Use as Calpain Inhibitors V. *WO 2013149800*, 2013.

(60) Kling, A.; Mack, H.; Jantos, K.; Moeller, A.; Hornberger, W.; Hutchins, C. W. Carboxamide Compounds and Their Use as Calpain Inhibitors. *WO 2010094755*, 2010.

(61) Kim, Y. B.; Kopcho, L. M.; Kirby, M. S.; Hamann, L. G.; Weigelt, C. A.; Metzler, W. J.; Marcinkeviciene, J. Mechanism of Gly-Pro-pNA Cleavage Catalyzed by Dipeptidyl Peptidase-IV and its Inhibition by Saxagliptin (BMS-477118). *Arch. Biochem. Biophys*. **2006**, *445*, 9-18.

(62) Nimmrich, V.; Reymann; K. G.; Strassburger, M.; Schöder; U. H.; Gross, G.; Hahn, A., Schoemaker, H., Wicke, K.; Möller, A. Inhibition of Calpain Prevents NMDA-induced Cell Death and beta-Amyloid-induced Synaptic Dysfunction in Hippocampal Slice Cultures. *Br. J. Pharmacol*. **2010**, *159*, 1523–1531.

Table of Contents Graphic

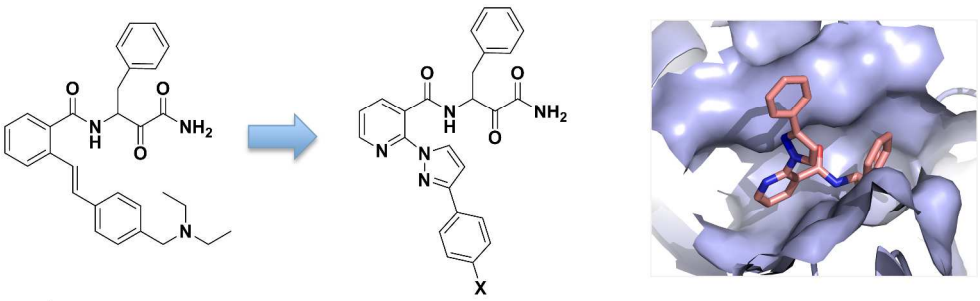

1
Ki Cal1 = 56 nM

Low selectivity
vs. cysteine protease cathepsins

X = H 19: Ki Cal1 = 18 nM
X = F 38: Ki Cal1 = 34 nM

High selectivity
vs. cysteine protease cathepsins